

Nanocrystal Patterning

Zitierweise: *Angew. Chem. Int. Ed.* **2022**, *61*, e202202633

Internationale Ausgabe: doi.org/10.1002/anie.202202633

Deutsche Ausgabe: doi.org/10.1002/ange.202202633

Beyond a Linker: The Role of Photochemistry of Crosslinkers in the Direct Optical Patterning of Colloidal Nanocrystals

Shaoyong Lu⁺, Zhong Fu⁺, Fu Li, Kangkang Weng, Likuan Zhou, Lipeng Zhang, Yuchen Yang, Hengwei Qiu, Dan Liu, Wenyue Qing, He Ding, Xing Sheng, Menglu Chen, Xin Tang, Lian Duan, Wenyong Liu, Longjia Wu, Yixing Yang, Hao Zhang,* and Jinghong Li

Abstract: Surface chemistry mediated direct optical patterning represents an emerging strategy for incorporating colloidal nanocrystals (NCs) in integrated optoelectronic platforms including displays and image sensors. However, the role of photochemistry of crosslinkers and other photoactive species in patterning remains elusive. Here we show the design of nitrene- and carbene-based photocrosslinkers can strongly affect the patterning capabilities and photophysical properties of NCs, especially quantum dots (QDs). Their role beyond physical linkers stems from structure-dictated electronic configuration, energy alignment and associated reaction kinetics and thermodynamics. Patterned QD layers with designed carbene-based crosslinkers fully preserve their photoluminescent and electroluminescent properties. Patterned light emitting diodes (QLEDs) show a maximum external quantum efficiency of $\approx 12\%$ and lifetime over 4800 h, among the highest for reported patterned QLEDs. These results would guide the rational design of photoactive species in NC patterning and create new possibilities in the monolithic integration of NCs in high-performance device platforms.

Introduction

Colloidal nanocrystals (NCs) constitute an emerging class of materials for building next-generation electronic, optoelectronic, and photonic devices.^[1] Advances in the chemistry of NC cores and surface ligands as well as in the engineering of device structures have led to materials and prototype devices with performance approaching those of traditional inorganic and organic counterparts.^[1a,c] Effective patterning of NCs with microscale precision represents a critical step toward the system-level integration of NC-based devices and their commercial applications in consumer electronics and advanced optics, including high-definition displays, image sensor arrays and wearable devices.^[1a,2]

Ideal patterning methods for NCs should afford high-resolution patterning in a high-throughput manner and support the fabrication of high-performance integrated devices. Due to the surface-dictated properties of NCs, it is extremely challenging to achieve desirable patterning capabilities while preserve the physical and chemical properties of NCs. Conventional methods, such as photolithography,^[3] transfer-printing^[4] and ink-jet printing,^[5] typically suffer from their modest compatibility with NCs and/or discrepancies between the original designs and obtained pixel geometries.^[2,6] For instance, photoresists and solvents used in traditional photolithography interact with NCs in a complex way that usually degrades the photophysical properties of NCs.^[3a] Recently, Talapin group developed a new patterning strategy featuring the photoresist-free, direct optical lithography of NCs.^[7] This concept relies on the unique surface ligand chemistry of NCs and thus represents

[*] Dr. S. Lu,⁺ Z. Fu,⁺ Dr. F. Li, Dr. K. Weng, Dr. L. Zhang, Y. Yang, Dr. H. Qiu, D. Liu, W. Qing, Prof. L. Duan, Prof. H. Zhang, Prof. J. Li

Department of Chemistry, Key Laboratory of Bioorganic Phosphorus Chemistry and Chemical Biology, Ministry of Education, Center for BioAnalytical Chemistry, Tsinghua University Beijing 100084 (China)

E-mail: hzhangchem@mail.tsinghua.edu.cn

L. Zhou, Dr. W. Liu, Dr. L. Wu, Dr. Y. Yang
TCL Research, No. 1001 Zhongshan Park Road
Shenzhen, Guangdong 518067 (China)

Prof. H. Ding
Beijing Engineering Research Center of Mixed Reality and Advanced Display, School of Optics and Photonics,
Beijing Institute of Technology
Beijing 100081 (China)

Prof. X. Sheng
Department of Electrical Engineering, Beijing National Research Center for Information Science and Technology,
Tsinghua University
Beijing 100084 (China)

Prof. M. Chen, Prof. X. Tang
Beijing Key Laboratory for Precision Optoelectronic Measurement Instrument and Technology, School of Optics and Photonics,
Beijing Institute of Technology
Beijing 100081 (China)

Prof. X. Sheng, Prof. L. Duan, Prof. H. Zhang
Center for Flexible Electronic Technology,
Tsinghua University
Beijing 100084 (China)

[†] These authors contributed equally to this work.

a more material-adapted patterning strategy. Inspired by this work, a series of photoactive species were introduced to NC inks as additives or ligands, leading to prototype pixelated NC devices.^[8] Among these, Kang and co-workers reported the direct optical patterning of semiconducting NCs (or quantum dots, QDs) via light-driven crosslinking of their native ligands under deep UV (254 nm) irradiation.^[9] This method uses nonspecific bisazide/nitrene-based crosslinkers and produces high-resolution, microscale pixelated QD layers with largely maintained photoluminescent (PL) and electroluminescent (EL) characteristics. Despite the encouraging progress in the direct optical patterning of NCs, the role of the photochemistry of these photoactive additives/ligands remains largely unexplored. For instance, the nitrene-based crosslinkers were treated mainly as physical linkers to bond adjacent NCs.^[9] Analogous to the importance of ligand chemistry in governing NC properties,^[10] it is conceivable that the chemistry of photocrosslinkers and other photoactive species is crucial to the properties of patterned NCs and associated devices.

In this work, we elaborate the role of photochemistry of nitrene- and carbene-based crosslinkers in the direct optical patterning of NCs. These molecules, far beyond physical linkers, strongly affect both the patterning capabilities and the photophysical properties of patterned NCs and devices. These can be traced to their molecular designs and associated changes in light absorption properties, electronic structures, spin states, and reaction pathways. Rationally designed nitrene- and carbene-based crosslinkers enable high-fidelity NC patterning at near UV (i-line, 365 nm) with low doses (<50 mJcm⁻²). The formed patterns show high lateral resolution approaching the limit of the photomasks ($\approx 3 \mu\text{m}$ in our case) and low surface roughness (about the height of a single NC). Moreover, the photochemistry of crosslinkers remarkably affects the PL and EL properties of NCs. Crosslinkers with extended spectral response (365 versus 254 nm) are preferred for the preservation of PL quantum yields (PLQYs) of patterned QD layers and external quantum efficiency (EQE) of associated patterned QD light emitting diodes (QLEDs). The newly developed carbene-based crosslinkers show proper electronic energy alignment with QDs and benign photochemistry during patterning. Compared to nitrene-based ones, they enable nondestructive QD patterning with significantly higher retention in PLQYs ($\approx 90\%$ relative to initial values). These crosslinkers also yield patterned QLEDs with fully preserved EL characteristics, featuring decent EQE (11.7%) and long operating lifetime (T_{95} at 1000 nit ≈ 4800 h). Both are on par with the highest values for patterned QLED devices. Additionally, the photocrosslinking chemistry can nicely integrate with previously developed ligand exchange chemistry and enable patterned NC devices with improved electronic communication. Results shown here highlight the importance of photochemistry of crosslinkers, and more generally photoactive species, in the direct optical patterning of NCs. The correlation between the photochemistry of photoactive species and photophysics of NCs revealed here will guide the rational design of direct optical patterning

strategies for building high-performance, integrated NC optoelectronic platforms for widespread technologies.

Results and Discussion

The Role of Photochemistry of Crosslinkers in the Patterning Capabilities of NCs

Figure 1A shows the molecular structures of four representative photocrosslinkers used in this work. These include (1*E*,4*E*)-1,5-bis(4-azido-2,3,5,6-tetrafluorophenyl)penta-1,4-dien-3-one (**1**), ethylene bis(4-azido-2,3,5,6-tetrafluorobenzoate) (**2**), (3*E*,5*E*)-3,5-bis(4-azido-2,3,5,6-tetrafluorobenzylidene)-1-methylpiperidin-4-one (**3**), and 3,3'-(4,4'-(perfluorobutane-1,4-diyl) bis(4,1-phenylene)) bis(3-(trifluoromethyl)-3H-diazirine) (**4**). Their synthesis and nuclear magnetic resonance (NMR) spectra appear in Schemes S1–S4 and Figures S1–S4. All these crosslinkers are stable during long-term storage in the absence of light. Crosslinkers **1–3** contain bis(perfluorophenyl) azide (bisPFPA) motifs and serve as light-activatable nitrene precursors while the diazine-containing crosslinker **4** readily generates phenyl carbene radicals upon photochemical stimulation. These molecules have been used as sensitizers in conventional photoresists,^[11] photo affinity labeling reagents in biochemistry,^[12] and more recently, crosslinkers for functional polymers.^[13] Among them, **2** has been reported as an effective photocrosslinker for QD patterning at 254 nm^[9] and serves as a benchmark in this study. In comparison, carbene-based crosslinkers are firstly reported for NC patterning in this work, expanding the toolbox of direct optical patterning. Figure 1B depicts the general patterning mechanism. Under UV irradiation, the photolysis of **1–4** releases nitrogen and produces highly reactive singlet nitrene or carbene intermediates at both ends. These radicals readily undergo nonspecific C–H insertion with the native, alkyl ligands of NCs and covalently bond neighboring NCs. These crosslinking events substantially reduce the solubility/redispersability of NCs in the exposed regions in their original nonpolar solvents. This process sets the foundation for patterning. This assumption can be validated by the loss of colloidal stability of a NC ink containing crosslinkers after UV irradiation (Figure 1C). Accordingly, direct optical patterning of NCs can be achieved following procedures shown in Figure 1D, including the film coating of a mixture of NCs and crosslinkers, UV irradiation at selected regions via a photomask, and removal of unexposed parts with developer solvents (common nonpolar solvents in this case).

Beyond the role as a crosslinker shown in Figure 1B, the photochemistry of **1–4** strongly affects the patterning capabilities of NCs. To demonstrate this, we used red-emitting II–VI based core/shell QDs and CdSe NCs with conventional oleic acid and oleylamine ligands as model systems. Their morphological and optical properties are shown in Figure S5. Figures 2A,B show the schemes of the photogeneration of nitrene and carbene radicals, the equilibria between different spin states, the kinetics in C–H

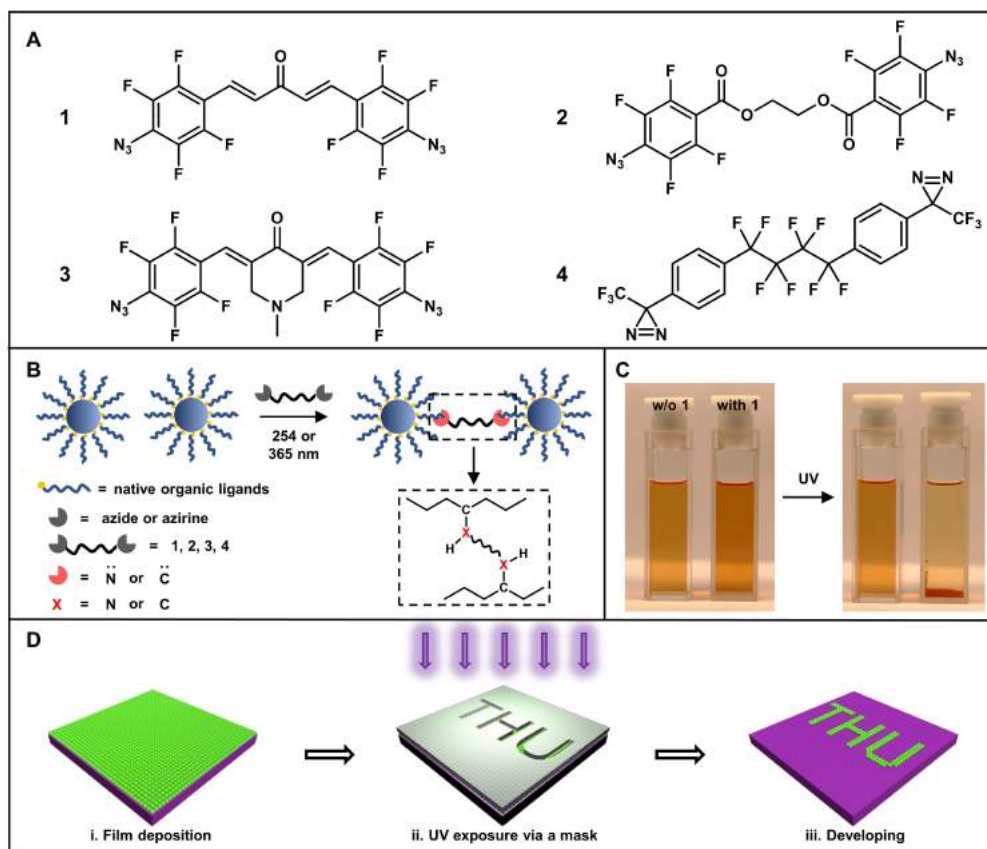


Figure 1. Scheme and procedures for direct optical patterning of NCs with photocrosslinkers. A) Molecular structures of four photocrosslinkers. B) Patterning mechanism. Photogenerated nitrene- and carbene-based crosslinkers bridge native ligands on adjacent NCs via C–H insertion. C) Photographs of CdSe NCs in 1,1,2-trichlorotrifluoroethane with and without (w/o) crosslinker **1** before and after UV exposure. In the presence of crosslinkers, NCs lose colloidal stability after UV exposure. D) Patterning procedures, including i) deposition of films containing NCs and crosslinkers, ii) UV exposure via a mask, and iii) developing.

insertion, and the side reactions with oxygen. Details of these reaction pathways were thoroughly studied by Platz, Keana, Sander and other groups and accounted elsewhere.^[14] The core difference in nitrene and carbene photochemistry is their “open shell” versus “closed shell” electronic configurations (highlighted in dashed boxes in Figures 2A, B). This causes drastically dissimilar thermodynamics and kinetics in the above photochemical reactions^[14b] that are responsible for the structure–function relationship of crosslinkers in NC patterning capabilities and photo-physical properties, as discussed below.

The first step involved in the photochemistry of crosslinkers is their photolysis at specific wavelengths. Changing the linkers between the two PFFPA groups in **1–3** shifts the maximum absorption peaks to longer wavelengths (Figure 2C). The absorption wavelengths and molar extinction coefficients (ϵ) define the efficiency in the photolysis of bisPFPAs and thus the patterning capabilities. Crosslinkers with higher ϵ are preferred considering the large optical absorption cross-section of QDs (typically in the range of 10^5 – 10^6 $\text{cm}^{-1}\text{M}^{-1}$ in the UV region^[15]) (Figure S6). Crosslinker **2** has a high $\epsilon \approx 3.6 \times 10^4$ $\text{cm}^{-1}\text{M}^{-1}$ at ≈ 260 nm but no absorption beyond 300 nm. **1** and **3** show red-shifted

absorption peaks with lower ϵ at 365 nm, $\approx 1.2 \times 10^4$ and $\approx 0.36 \times 10^4$ $\text{cm}^{-1}\text{M}^{-1}$, respectively. The patterning capabilities of **1–3** at 365 nm correlate well with the trend in ϵ . As shown in Figure 2D, exposing films containing both NCs and **2** at 365 nm (3 wt % of **2** relative to the mass of NCs, 1.7 mW cm^{-2} for 30 s, or 50 mJ cm^{-2}) forms no noticeable red QD patterns. Patterning with **1** under otherwise the same condition yields high-fidelity patterns. In comparison, **3** produces patterns with poor film quality under similar condition or even with prolonged exposure (200 mJ cm^{-2}), probably due to the low ϵ and insufficient supply of nitrene radicals.

Compared to bisPFPAs, the diazirine-based crosslinker **4** shows almost two orders of magnitude lower ϵ ($\approx 3.0 \times 10^2$ $\text{cm}^{-1}\text{M}^{-1}$) at 365 nm. However, they produce high quality QD patterns (Figure 2D) with comparable UV doses (200 mJ cm^{-2}) and crosslinker contents (6 wt %). Note we used the weight ratio (instead of molar ratio) for all crosslinkers for convenience in comparison as the molecular weights of all crosslinkers are similar, ranging from ≈ 460 to 570 g mol^{-1} . The contrast in the efficiency of two types of radicals in NC patterning coincides with the significantly faster kinetics of carbene in C–H insertion (the key step for

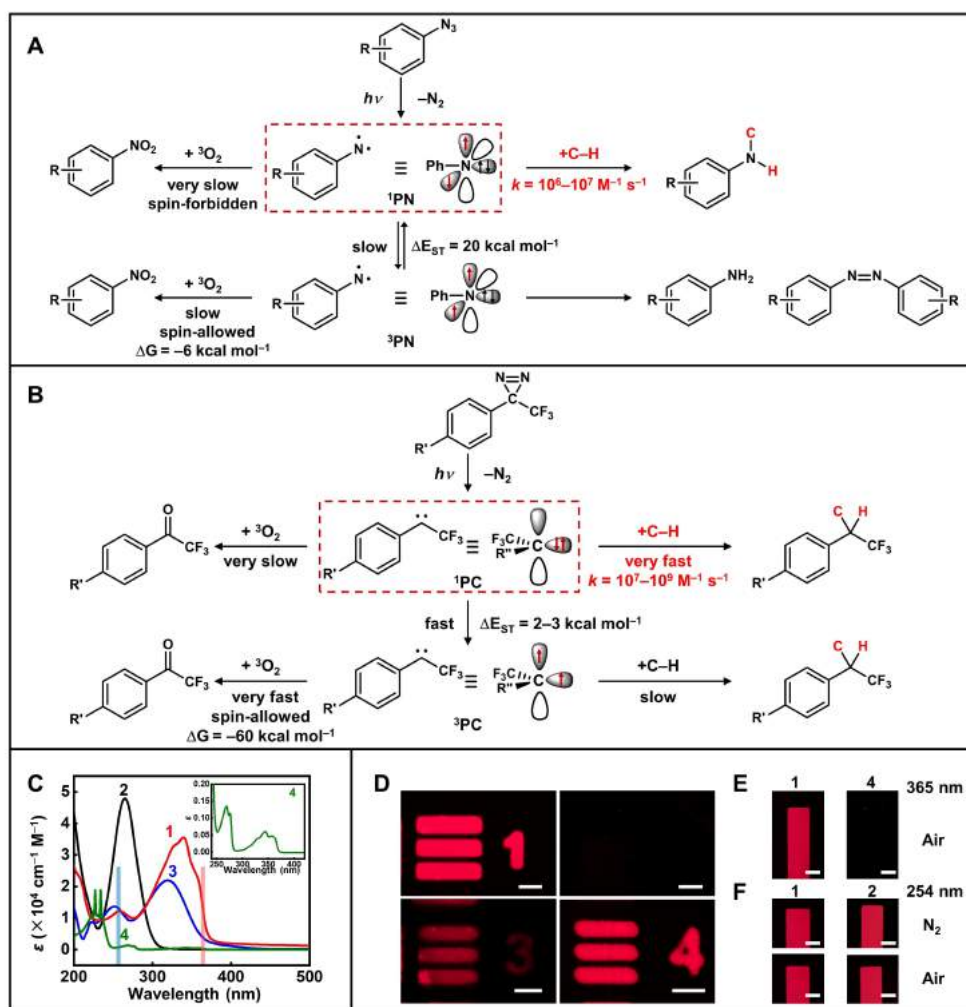


Figure 2. The role of photochemistry of crosslinkers in the patterning capabilities. A), B) Schemes of the photochemistry of crosslinkers, including the photogeneration of nitrene and carbene radicals, the electronic configurations, the kinetics in C–H insertion, the equilibria between different spin states, and the side reactions with oxygen. C) ϵ of four crosslinkers in acetonitrile. Shaded bars in (C) indicate wavelengths near 254 and 365 nm. Inset shows ϵ ($\times 10^4 \text{ cm}^{-1} \text{ M}^{-1}$) of crosslinker 4. D)–F) Fluorescence optical microscopic images of patterned red QD layers under different conditions. D) with crosslinkers 1–4 (as indicated by the numbers in the patterns; 2 forms no patterns) at 365 nm in N_2 , E) with 1 and 4 at 365 nm in air, and F) with 1 and 2 at 254 nm in N_2 or air. Scale bars in (D): 30 μm , (E), (F): 100 μm .

NC crosslinking) compared to nitrene, primarily due to their different electronic configurations (Figures 2A,B).^[14b,16] i) The sp^2 -hybridization of singlet phenyl carbene (1PC) and other factors favor the σ^2 -configuration of the two electrons in the same orbital. In these “closed-shell” singlet states, the empty p - π -orbitals facilitate the rapid addition to C–H bonds through a concerted pathway. By contrast, the sp -hybridization of singlet phenyl nitrene (1PN) leads to the $\sigma^1\pi^1$ -configuration with two electrons in different p -orbitals and with opposite spin directions. These “open-shell” structures cannot afford C–H insertion events at rates on par with singlet carbene (2–3 orders of magnitude lower).^[14a,17] ii) The intersystem conversion between spin states also contributes to the difference in the reaction kinetics. The small energy gap for intersystem conversion ($\Delta E_{ST} \approx 2-3 \text{ kcal mol}^{-1}$, Figure 2B, insensitive to the substituents in the phenyl ring^[18]) suggests that singlet and triplet

phenyl carbene radicals equilibrate rapidly at ambient temperature; triplet carbene can serve as a reservoir for highly reactive singlet carbene.^[14b] The large ΔE_{ST} for aryl nitrene ($\approx 20 \text{ kcal mol}^{-1}$) discourages this conversion and triplet nitrene radicals typically convert to amines or azo-compounds.^[12,13d,14f] These factors render **4** more efficient toward C–H insertion, compensating the limited supply of carbene radicals due to the low ϵ .

The efficient crosslinker **4**, however, becomes less effective when used in the air (Figure 2E), even with significantly prolonged exposure (over 1000 mJ cm^{-2}). On the contrary, nitrene-based crosslinkers (e.g., **1** and **2**) remain effective regardless of the environment (Figure 2F). The sensitivity of patterning capabilities to air can also be explained by their photochemistry illustrated in Figures 2A,B. Oxygen with a triplet ground state (3O_2) can react with both triplet nitrene and carbene radicals following the

spin selection rule, but at different rates. Triplet carbene reacts much more rapidly with oxygen, approaching the diffusion control, than does with triplet nitrene. The notably different kinetics is due to the large discrepancy in the changes in free energy during oxidation ($\Delta G \approx -60$ versus -6 kcal mol⁻¹ for carbene and nitrene, respectively).^[14d,e] Therefore oxygen is a major quencher of photogenerated carbene radicals while the much slower oxidation of nitrene only moderately reduces the C–H insertion rates, reported as the “reciprocity failure” in conventional photoresists.^[11b] One possible solution to the air-sensitivity of phenyl carbene-based crosslinkers is to switch their ground state to singlet (unreactive to ³O₂) by substitution of the aromatic ring, as predicted by Wulff and co-workers.^[16b] It is also important to note recent studies on the patterning of functional polymers with carbene-based crosslinkers did not specify the required atmosphere for patterning.^[13a,b]

The above results show the photochemical origin of the modulated patterning capabilities of NCs in a qualitative way. Moreover, we used film retention, defined as the percentage of NCs remained in the crosslinked (patterned) film after solvent developing and measured by inductively coupled plasma-optical emission spectrometry (ICP-OES), for a quantitative estimation of the patterning quality. Film retention is highly reliant on the UV exposure doses, the contents of crosslinkers, and the ratio between crosslinkers and NC ligands. Zinc blende CdSe NCs with solely oleic

acid ligands, together with crosslinker **1**, serve as an example for this analysis. Details appear in the Supporting Information (Supporting Information Discussion 1 and Figures S7, S8). With only 5–10 mol% of crosslinkers (relative to the number of ligands) and a dose of 50 mJ cm⁻², crosslinked NC layers show both high film retention ($\approx 75\%$) and high patterning quality. Figure 3 shows representative QD patterns formed with **1** at 365 nm under optimized conditions. Scanning electron microscopic (SEM) and optical fluorescent images (Figures 3A,B) show patterned QD layers in the formats of complex logos and uniform arrays of geometric shapes. Using well-established infrastructures in conventional photolithography, microscale QD patterns with resolution of $\approx 3 \mu\text{m}$ are obtained, replicating that of the predesigned photomasks (Figure 3C). The height profiles confirm the uniform and adjustable thickness of patterned QD layers (Figure 3D). The line profiles measured by both the profilometer and atomic force microscopy (AFM) (Figure 3E) reveal the sharp and well-defined edges without traces of capillary meniscus. AFM images (Figure 3F,G) also provide direct comparison in the quality of pristine and patterned/crosslinked QD films, suggesting no changes in the averaged surface roughness (≈ 2.80 nm, smaller than the size of a single QD) and morphology. The top-view SEM image (Figure 3H) corroborates with the AFM analysis, showing closely packed QDs without noticeable pinholes or cracks. **1** also affords high-quality patterned

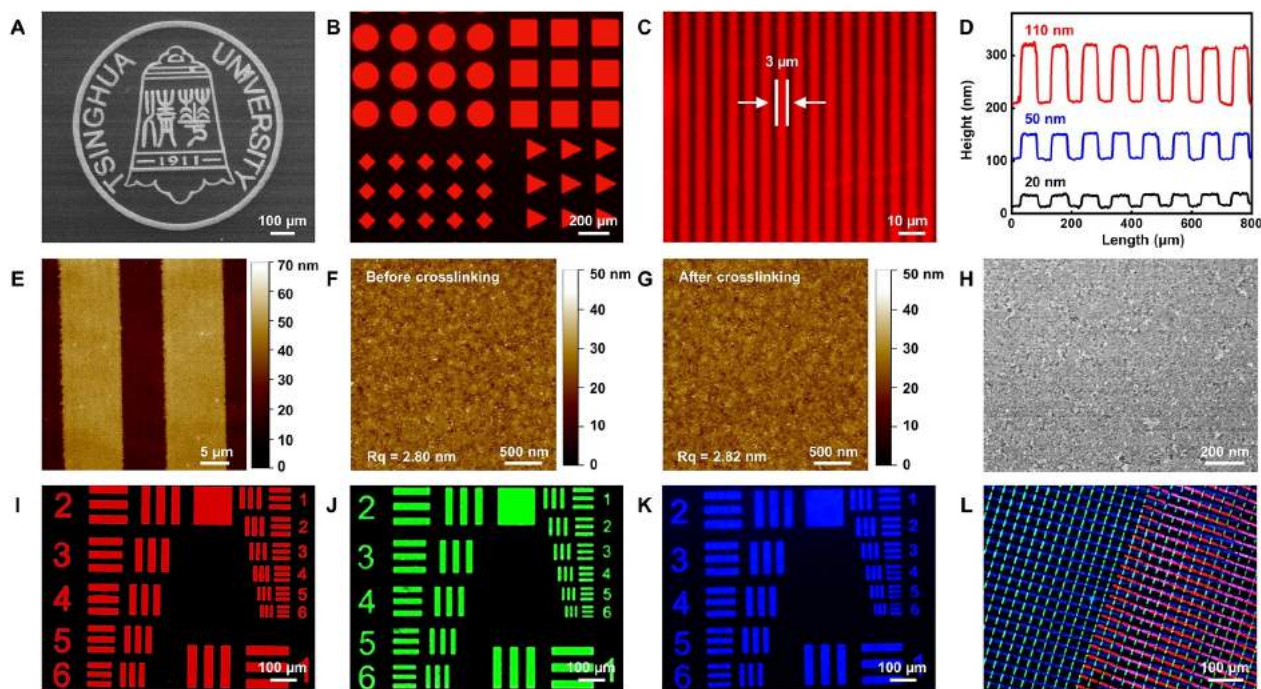


Figure 3. Optical and microscopic images of patterned QD layers with crosslinker **1** at 365 nm. A) SEM image of patterned QDs in the shape of Tsinghua logo. B), C) Fluorescent microscopic images of QD patterns as arrays of geometric shapes and uniform lines. D) Height profiles of line patterns with different thickness. E)–G) AFM images of line patterns (E) and the surface roughness analysis of QD films before (F) and after (G) crosslinking. H) Top-view SEM image of patterned QD layer. I)–K) Fluorescent microscopic images of patterned red, green, and blue QD layers in the format of 1951 U.S. Air Force target. L) Fluorescent microscopic image of triple-layered, cross-line patterns. Typical patterning condition: 3 wt% of **1**, and UV dose of 50 mJ cm⁻² at 365 nm.

layers of red, green, and blue QDs in a sequential, layer-by-layer fashion (Figures 3I–L), as highlighted by the triple layered cross-line images. Each rectangular subpixel in Figure 3L has the dimension of $5 \times 25 \mu\text{m}$. Additional SEM images are shown in Figure S9. Similarly, patterning with carbene-based crosslinker **4** at 365 nm also produces high quality QD patterns (Figure S10).

The Role of Photochemistry of Crosslinkers in the PL and EL Characteristics of NCs

Rather than inert, physical linkers, crosslinkers used in NC patterning are well-known, highly reactive intermediates. The interplay of the rich photochemistry of crosslinkers and the sensitive surface chemistry of NCs (especially QDs) remains largely uncharted. We selected nitrene- and carbene-based crosslinkers (**1**, **2**, **4**) as examples to build the connection between the optical, electronic and photochemical properties of crosslinkers and the photophysics of patterned QDs (red-emitting core/shell CdZnSe/CdZnS/ZnS with initial PLQYs of $\approx 60\%$). Crosslinkers with extended response to light with longer wavelengths, proper electronic energy levels, and benign photochemistry are favored for better PL and EL properties of patterned QDs and associated devices, as discussed below.

The dual absorption features with almost identical ϵ ($\approx 1.2 \times 10^4 \text{ cm}^{-1} \text{ M}^{-1}$) at 254 and 365 nm endow **1** with the capability to effectively pattern QDs at both wavelengths (Figures 2E,F). Despite the similar quality of obtained patterns, the two patterning wavelengths (or photon energy) introduce notably different effects on the PL properties. To evaluate this, we monitored the PLQYs and time-resolved PL spectra of QD films at various stages of patterning (Figure 4). These stages include pristine, UV exposure (without crosslinkers), formulation (films containing both QDs and crosslinkers prior to exposure), and patterned (photocrosslinked films in the presence of both UV exposure and crosslinkers, followed by developing). QD films largely retain their PLQYs (96% relative to their original value, Figure 4A) after exposed for 50 mJ cm^{-2} at 365 nm. By contrast, similar UV doses (50 mJ cm^{-2}) at 254 nm decrease PLQYs by about 40%. Changes in the averaged PL lifetime (Table S1) corroborate the trend in PLQYs. The reduction in PLQYs is more pronounced for patterned QD films. The 365 nm-patterned QD layers maintain 55% of the original PLQY with a much reduced averaged lifetime (from 21.1 to 15.1 ns, Figure 4B and Table S1). The 254 nm-patterned samples show notably lower relative PLQY ($\approx 38\%$) and an even shorter averaged PL lifetime of 13.5 ns. This clearly shows the advantage of patterning QDs at longer wavelengths, which is linked to the intrinsic photostability of QDs. Significant reduction in PLQYs ($\approx 42\%$ relative to pristine samples) was also observed for films patterned with **2** at 254 nm. This observation is different from the recently reported non-destructive QD patterning with **2**, showing no noticeable changes in PLQYs.^[9] We note the contents of crosslinkers and UV doses used in their work ($\approx 2 \text{ wt}\%$ of **2** and

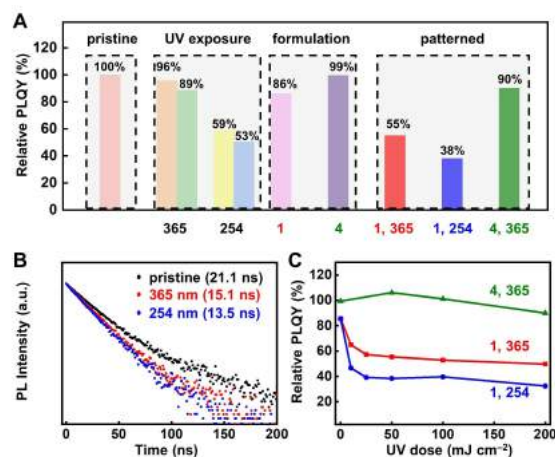


Figure 4. PL characteristics of patterned QDs with different crosslinkers. A) Relative PLQYs of QD films at various stages of patterning: Pristine, UV exposure (under 365 and 254 nm, without crosslinkers; for each wavelength, the left column represents doses of 50 mJ cm^{-2} and the right column represents 200 mJ cm^{-2}), formulation (films containing QDs and 3 wt% of crosslinker **1** or 6 wt% of **4**), and patterned (3 wt% of **1** and 50 mJ cm^{-2} at 365 or 254 nm and 6 wt% of **4** and 200 mJ cm^{-2} at 365 nm, followed by developing). B) PL decay curves of pristine and patterned QD films with **1** under 254 and 365 nm. The averaged lifetime from data fitting is shown in the parentheses. C) Changes in relative PLQYs for QD films with **1** and **4** at different doses.

$\approx 2 \text{ mJ cm}^{-2}$ at 254 nm) were remarkably lower. These may arise from the variations in the core and surface properties of starting QDs, which also underlines the importance of studying the relation between the photochemistry of crosslinkers and the properties of patterned QDs.

In parallel to the wavelength-dependent photostability of QDs, the molecular design of crosslinkers strongly affects the PL properties both electronically and photochemically. QD films crosslinked with nitrene-based **1** and carbene-based **4**, both at 365 nm, show drastically different PLQYs (Figure 4A). The latter is almost nondestructive compared to the former (relative PLQY $\approx 90\%$ versus 55%) even with a prolonged UV dose (200 versus 50 mJ cm^{-2}). The slightly decreased PLQYs for carbene-crosslinked QDs are mainly due to the modest photodegradation under 365 nm exposure. The combination of ultraviolet photoelectron spectroscopy (UPS) and UV/Visible absorption spectra allows the estimation of the highest occupied molecular orbitals (HOMO) and lowest unoccupied molecular orbitals (LUMO) of **1** and **4**. Figure S11 shows the schematic electronic energy alignment of QDs,^[19] **1**, and **4**. The LUMO of **1** is within the band gap of cores of QDs (i.e., **1** has higher electron affinity than QDs) and can thus accept their photogenerated carriers (electrons).^[19] This charge transfer process can explain the decreased PLQY at the formulation stage of **1**. In comparison, **4** holds HOMO and LUMO levels mostly outside those of CdSe cores and thus introduce neither carrier nor exciton traps.

The divergence in PLQYs for nitrene (**1**)- and carbene (**4**)-photocrosslinked QD films significantly increases from

the formulation stage (86 % versus 99 %) to the patterned stage (55 % versus 90 %). This confirms the importance of photochemistry of crosslinkers. The photochemical effect can be rationalized from the perspective of reaction kinetics and pathways of nitrene and carbene radicals. Figure 4C shows the changes in PLQYs of patterned QDs as a function of UV doses with **1** at both 254 and 365 nm. PLQYs decrease in both cases with extended UV exposure and the major loss occurs at doses relevant to the patterning condition ($< 100 \text{ mJ cm}^{-1}$). The PLQY changes coincide with the photolysis of **1** and the generation of nitrene radicals, as monitored by Fourier transformed infrared (FTIR) spectra (Figure S12). The sharp decline in the absorption of azido group ($-\text{N}_3$, $\approx 2100 \text{ cm}^{-1}$) at early stage of UV exposure suggests the burst of nitrene radicals and synchronizes with the drops in PLQYs. Compared to 254 nm, 365 nm irradiation generates nitrene radicals at smaller rates and causes smaller reduction in relative PLQYs. The correlation of PLQY decreases with nitrene generation suggests excess nitrene radicals may be detrimental to QDs, in line with that conjectured in an earlier report.^[9] Both the radicals and the photogenerated byproducts might interact with QD surface in a complex manner (Supporting Information Discussion 2). These reduced PLQYs can be further related to the increased density of surface defects during the patterning stages, as indicated by the increased nonradiative recombination rates (Table S1). By contrast, carbenes have been reported as Lewis bases/ligands that are able to stabilize Cd^{2+} or Zn^{2+} -metal complexes^[20] and passivate II–VI QDs.^[21] Unraveling the nature of the photochemical effects of nitrene- and carbene-based crosslinkers needs further studies. Nonetheless, the combination of the benign photo-

chemistry of carbene radicals and the high photostability of QDs against 365 nm exposure leads to almost unchanged PLQYs and thereby nearly nondestructive patterning (Figure 4C).

The choice of crosslinkers also affects the EL characteristics of QLEDs with patterned QD active layers. Figures 5A,B show the device structure and energy level diagram of the fabricated QLEDs. We compared the EL performance of both pristine and patterned devices. Details about device fabrication appear in the Supporting Information. The EL spectra of patterned QLEDs with different combinations of crosslinkers and exposure wavelengths remain unchanged relative to the pristine devices (Figure S13). Figures 5C,D compare the current density–voltage–luminance (J – V – L) characteristics of typical pristine and 365 nm-patterned devices. The results are from two different batches of measurements and the performance for pristine devices are slightly different. Nonetheless, both pristine and patterned devices show decent performance with EQEs in the range of 11–13 % (Figure S13 and Table S2), on par with the record EQEs (14.6 %^[9]) reported for patterned QLEDs by direct optical patterning strategy. Note standard and inverted device structures were used here and in earlier work,^[9] respectively. Similar to the trend observed in PL properties, patterning at 365 nm is preferred in retaining the high EQEs and brightness. For instance, devices patterned with **1** at 365 nm preserve ≈ 94 % of the EQEs of pristine ones (Figure 5E), comparing favorably with those of 254 nm-patterned devices with either **1** or **2** (≈ 86 % and ≈ 90 % relative to pristine devices), although the difference is not as significant as that in the PL cases. Carbene-based **4** remains nondestructive and affords patterned devices show-

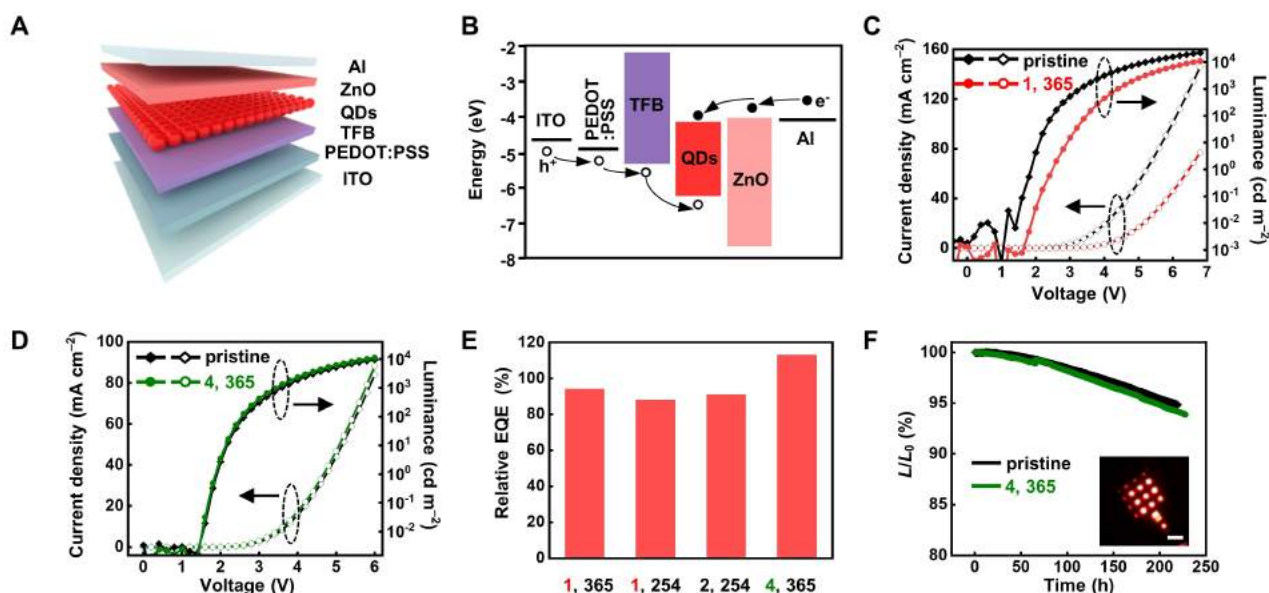


Figure 5. EL characteristics of pristine and patterned QLEDs with different crosslinkers. A), B) Device structure and energy level diagram of the fabricated QLEDs. C), D) Current density–voltage–luminance (J – V – L) characteristics of pristine and patterned devices (365 nm). C) with 5 wt % of **1** and 50 mJ cm^{-2} and D) with 10 wt % of **4** and 200 mJ cm^{-2} . E) Summary of relative EQEs of QLEDs compared to corresponding pristine devices under different patterning conditions (crosslinkers and wavelengths). F) Temporal changes in relative luminance (L/L_0) of pristine and patterned QLEDs (with **4** at 365 nm). Inset shows an EL image of a patterned pixelated device (scale bar: 1 mm).

ing almost identical EQEs and maximum luminance with those of pristine devices (Figure 5E, Table S2). The full retention of EL performance presumably originates from a combination of the mild photochemistry and benign electronic structures of **4**. More remarkable difference was observed in the device operating lifetime. The temporal changes in luminance of patterned devices (with **4**) resemble those of pristine ones (Figure 5F). Their T_{95} (or the time for the luminance to drop to 95 % of its original value, ≈ 190 h) exceeds those reported for nitrene-crosslinked QLEDs (in the order of 10 h^[9]). The extrapolated T_{95} at 1000 nit (i.e., at an initial brightness of 1000 cd m⁻²) is over 4800 h (pristine devices ≈ 4100 h), on par with those of the state-of-the-art QLED devices.^[22] In comparison, devices patterned with nitrene-based **1** and **2** show notably reduced T_{95} (≈ 50 % compared to the values of pristine devices, Table S2). Although the origin of the observed differences in EL properties with different crosslinkers and wavelengths need more in-depth study (e.g., single carrier device measurements), the high EQEs, brightness and operating lifetime suggest the potential of photocrosslinking approach in fabricating high-performance and high-definition LED displays. As a proof of concept, we made pixelated patterns (EL images shown in the inset of Figure 5F).

Additionally, the photocrosslinking patterning approach relies on the reactions between nitrene or carbene radicals and the native surface ligands of NCs. It is applicable to a broad range of colloidal NCs with alkyl ligands, including metals, semiconductors (heavy metal-free InP, IR responsive PbS and HgTe, and CsPbBr₃ NCs), and magnetic materials (Figure S14A–E). More interestingly, this approach is fully compatible with previously reported ligand exchange chemistry for improved electronic communication.^[10a,b,23] Patterned Au NC films and HgTe NC based transistors, after post-patterning ligand exchange process, show decent conductivity and carrier mobility (Figure S14F–H). Details are shown in Supporting Information Discussion 3. The combination with post-patterning ligand exchange strategy extends the use of photocrosslinking-based patterning approach in building various integrated NC-based devices.

Conclusion

We have explored the role of the photochemistry of crosslinkers in the direct optical patterning of NCs. These results bridge the discerned patterning capabilities and photophysical properties to the underlying chemistry of nitrene- and carbene-based crosslinkers. Understanding their role beyond physical linkers guides the molecular design of crosslinkers that can support high-fidelity patterning of NC layers at 365 nm with fully preserved PL and EL properties. Prototype QLEDs patterned with carbene-based crosslinkers (**4**) show identical EQEs, luminescence and operating lifetime compared to their non-patterned counterparts. These EL characteristics (EQE ≈ 12 %, T_{95} at 1000 nit ≈ 4800 h) are on par with the records reported for QLEDs fabricated via direct optical patterning. It is conceivable that the advanced design of crosslinkers can yield patterned devices with

further improved performance. In addition, the photocrosslinking-based patterning approach is applicable to a broad scope of NCs and compatible with well-developed ligand exchange chemistry, yielding patterned devices with effective electronic communication. Results shown here have broad implications for the roles of photoactive species in NC patterning and stress the importance of photochemistry mindset in developing direct optical patterning strategies for NCs toward high-performance, integrated electronic and optoelectronic devices.

Acknowledgements

We thank W. Hang and Prof. C. Xi (Tsinghua) for help in the synthesis of crosslinkers. This work was financially supported by the National Natural Science Foundation of China (NSFC, grant no. 21974079). S.L. acknowledges support from the China Postdoctoral Science Foundation (no. 2020M680510) and the *Shuimu Tsinghua Scholar* Program. L. Zhou, W.L., L.W., Y.Y. acknowledge support from the Pearl River Talent Recruitment Program for Guangdong Introducing Innovative and Entrepreneurial Teams (2016ZT06C650). H. Ding acknowledges support from NSFC (no. 62005016).

Conflict of Interest

The authors declare no conflict of interest.

Data Availability Statement

The data that support the findings of this study are available from the corresponding author upon reasonable request.

Keywords: Optoelectronic Devices • Photo-Patterning of Nanocrystals • Photochemistry • Photocrosslinkers • Quantum Dots

- [1] a) F. P. García de Arquer, D. V. Talapin, V. I. Klimov, Y. Arakawa, M. Bayer, E. H. Sargent, *Science* **2021**, 373, eaaz8541; b) M. Liu, N. Yazdani, M. Yarema, M. Jansen, V. Wood, E. H. Sargent, *Nat. Electron.* **2021**, 4, 548–558; c) C. R. Kagan, E. Lifshitz, E. H. Sargent, D. V. Talapin, *Science* **2016**, 353, aac5523.
- [2] J. Yang, M. K. Choi, U. J. Yang, S. Y. Kim, Y. S. Kim, J. H. Kim, D.-H. Kim, T. Hyeon, *Nano Lett.* **2021**, 21, 26–33.
- [3] a) C. Hu, T. Aubert, Y. Justo, S. Flamee, M. Cirillo, A. Gassenq, O. Drobchak, F. Beunis, G. Roelkens, Z. Hens, *Nanotechnology* **2014**, 25, 175302; b) J.-S. Park, J. Kyhm, H. H. Kim, S. Jeong, J. Kang, S.-E. Lee, K.-T. Lee, K. Park, N. Barange, J. Han, J. D. Song, W. K. Choi, I. K. Han, *Nano Lett.* **2016**, 16, 6946–6953.
- [4] a) T.-H. Kim, K.-S. Cho, E. K. Lee, S. J. Lee, J. Chae, J. W. Kim, D. H. Kim, J.-Y. Kwon, G. Amaratunga, S. Y. Lee, B. L. Choi, Y. Kuk, J. M. Kim, K. Kim, *Nat. Photonics* **2011**, 5, 176–182; b) M. K. Choi, J. Yang, K. Kang, D. C. Kim, C. Choi, C.

- Park, S. J. Kim, S. I. Chae, T. H. Kim, J. H. Kim, T. Hyeon, D. H. Kim, *Nat. Commun.* **2015**, *6*, 7149.
- [5] G. Azzellino, F. S. Freyria, M. Nasilowski, M. G. Bawendi, V. Bulovic, *Adv. Mater.* **2019**, *31*, 1800727.
- [6] J. Zhao, L. Chen, D. Li, Z. Shi, P. Liu, Z. Yao, H. Yang, T. Zou, B. Zhao, X. Zhang, H. Zhou, Y. Yang, W. Cao, X. Yan, S. Zhang, X. W. Sun, *Nat. Commun.* **2021**, *12*, 4603.
- [7] Y. Wang, I. Fedin, H. Zhang, D. V. Talapin, *Science* **2017**, *357*, 385–388.
- [8] a) Y. Wang, J.-A. Pan, H. Wu, D. V. Talapin, *ACS Nano* **2019**, *13*, 13917–13931; b) H. Cho, J. A. Pan, H. Wu, X. Lan, I. Coropceanu, Y. Wang, W. Cho, E. A. Hill, J. S. Anderson, D. V. Talapin, *Adv. Mater.* **2020**, *32*, 2003805; c) J.-A. Pan, Z. Rong, Y. Wang, H. Cho, I. Coropceanu, H. Wu, D. V. Talapin, *J. Am. Chem. Soc.* **2021**, *143*, 2372–2383.
- [9] J. Yang, D. Hahm, K. Kim, S. Rhee, M. Lee, S. Kim, J. H. Chang, H. W. Park, J. Lim, M. Lee, H. Kim, J. Bang, H. Ahn, J. H. Cho, J. Kwak, B. Kim, C. Lee, W. K. Bae, M. S. Kang, *Nat. Commun.* **2020**, *11*, 2874.
- [10] a) M. A. Boles, D. Ling, T. Hyeon, D. V. Talapin, *Nat. Mater.* **2016**, *15*, 141–153; b) C. R. Kagan, C. B. Murray, *Nat. Nanotechnol.* **2015**, *10*, 1013–1026; c) C. R. Kagan, *Chem. Soc. Rev.* **2019**, *48*, 1626–1641; d) H. Zhang, K. Dasbiswas, N. B. Ludwig, G. Han, B. Lee, S. Vaikuntanathan, D. V. Talapin, *Nature* **2017**, *542*, 328–331.
- [11] a) S. Shimizu, G. R. Bird, *J. Electrochem. Soc.* **1977**, *124*, 1394; b) S. Shimizu, G. R. Bird, *J. Electrochem. Soc.* **1979**, *126*, 273.
- [12] J. F. W. Keana, S. X. Cai, *J. Org. Chem.* **1990**, *55*, 3640–3647.
- [13] a) Y.-Q. Zheng, Y. Liu, D. Zhong, S. Nikzad, S. Liu, Z. Yu, D. Liu, H.-C. Wu, C. Zhu, J. Li, H. Tran, J. B.-H. Tok, Z. Bao, *Science* **2021**, *373*, 88–94; b) C. Wu, C. Li, X. Yu, L. Chen, C. Gao, X. Zhang, G. Zhang, D. Zhang, *Angew. Chem. Int. Ed.* **2021**, *60*, 21521–21528; *Angew. Chem.* **2021**, *133*, 21691–21698; c) M. L. Lepage, C. Simhadri, C. Liu, M. Takaffoli, L. Bi, B. Crawford, A. S. Milani, J. E. Wulff, *Science* **2019**, *366*, 875–878; d) R.-Q. Png, P.-J. Chia, J.-C. Tang, B. Liu, S. Sivaramakrishnan, M. Zhou, S.-H. Khong, H. S. Chan, J. H. Burroughes, L.-L. Chua, R. H. Friend, P. K. H. Ho, *Nat. Mater.* **2010**, *9*, 152–158.
- [14] a) W. T. Borden, N. P. Gritsan, C. M. Hadad, W. L. Karney, C. R. Kemnitz, M. S. Platz, *Acc. Chem. Res.* **2000**, *33*, 765–771; b) M. S. Platz, *Acc. Chem. Res.* **1995**, *28*, 487–492; c) R. Poe, K. Schnapp, M. J. T. Young, J. Grayzar, M. S. Platz, *J. Am. Chem. Soc.* **1992**, *114*, 5054–5067; d) J. Liu, C. M. Hadad, M. S. Platz, *Org. Lett.* **2005**, *7*, 549–552; e) J. Mieres-Pérez, E. Mendez-Vega, K. Velappan, W. Sander, *J. Org. Chem.* **2015**, *80*, 11926–11931; f) M. Yan, S. X. Cai, M. W. Wybourne, J. F. Keana, *J. Mater. Chem.* **1996**, *6*, 1249–1252.
- [15] W. W. Yu, L. Qu, W. Guo, X. Peng, *Chem. Mater.* **2003**, *15*, 2854–2860.
- [16] a) N. P. Gritsan, A. D. Gudmundsdóttir, D. Tigelaar, Z. Zhu, W. L. Karney, C. M. Hadad, M. S. Platz, *J. Am. Chem. Soc.* **2001**, *123*, 1951–1962; b) S. F. Musolino, Z. Pei, L. Bi, G. A. DiLabio, J. E. Wulff, *Chem. Sci.* **2021**, *12*, 12138–12148; c) C. Simhadri, L. Bi, M. L. Lepage, M. Takaffoli, Z. Pei, S. F. Musolino, A. S. Milani, G. A. DiLabio, J. E. Wulff, *Chem. Sci.* **2021**, *12*, 4147–4153.
- [17] K. A. Schnapp, R. Poe, E. Leyva, N. Soundararajan, M. S. Platz, *Bioconjugate Chem.* **1993**, *4*, 172–177.
- [18] a) J. Mieres-Perez, P. Costa, E. Mendez-Vega, R. Crespo-Otero, W. Sander, *J. Am. Chem. Soc.* **2018**, *140*, 17271–17277; b) A. H. Raut, P. Costa, W. Sander, *Chem. Eur. J.* **2018**, *24*, 18043–18051.
- [19] a) H. Zhu, Y. Yang, H.-D. Kim, M. Califano, N. Song, Y. Wang, W. Zhang, O. V. Prezhdo, T. Lian, *Nano Lett.* **2014**, *14*, 1263–1269; b) H. Zhu, N. Song, T. Lian, *J. Am. Chem. Soc.* **2010**, *132*, 15038–15045.
- [20] H. Bauer, L. Orzechowski, A. Escalona, G. Jansen, S. Harder, *Organometallics* **2017**, *36*, 4883–4890.
- [21] a) L. Du, N. A. Nosratabad, Z. Jin, C. Zhang, S. Wang, B. Chen, H. Mattoussi, *J. Am. Chem. Soc.* **2021**, *143*, 1873–1884; b) D. E. Westmoreland, R. Lopez-Arteaga, E. A. Weiss, *J. Am. Chem. Soc.* **2020**, *142*, 2690–2696.
- [22] a) C. Xiang, L. Wu, Z. Lu, M. Li, Y. Wen, Y. Yang, W. Liu, T. Zhang, W. Cao, S. W. Tsang, B. Shan, X. Yan, L. Qian, *Nat. Commun.* **2020**, *11*, 1646; b) X. Dai, Z. Zhang, Y. Jin, Y. Niu, H. Cao, X. Liang, L. Chen, J. Wang, X. Peng, *Nature* **2014**, *515*, 96–99.
- [23] a) H. Zhang, J. Jang, W. Liu, D. V. Talapin, *ACS Nano* **2014**, *8*, 7359–7369; b) H. Zhang, J. M. Kurley, J. C. Russell, J. Jang, D. V. Talapin, *J. Am. Chem. Soc.* **2016**, *138*, 7464–7467; c) A. T. Fafarman, W.-K. Koh, B. T. Diroll, D. K. Kim, D.-K. Ko, S. J. Oh, X. Ye, V. Doan-Nguyen, M. R. Crump, D. C. Reifsnyder, C. B. Murray, C. R. Kagan, *J. Am. Chem. Soc.* **2011**, *133*, 15753–15761.

Manuscript received: February 17, 2022

Accepted manuscript online: March 23, 2022

Version of record online: April 5, 2022

Supporting Information

Beyond a Linker: The Role of Photochemistry of Crosslinkers in the Direct Optical Patterning of Colloidal Nanocrystals

S. Lu, Z. Fu, F. Li, K. Weng, L. Zhou, L. Zhang, Y. Yang, H. Qiu, D. Liu, W. Qing, H. Ding, X. Sheng, M. Chen, X. Tang, L. Duan, W. Liu, L. Wu, Y. Yang, H. Zhang, J. Li*

Table of Contents

1. Experimental Procedures
2. Supplementary Discussion
3. Supplementary Schemes (S1–S4), Figures (S1–S14), Tables (S1, S2)
4. References
5. Author Contributions

Experimental Procedures

1. Chemicals.

Cadmium oxide (CdO, 99.5%), trioctylphosphine oxide (TOPO, 90%), bis(trimethylsilyl) sulfide (>98%), borane tert-butylamine complex (97%), iron(III) chloride hexahydrate (99%), cesium carbonate (99.9%, trace metal basis), methyl acetate (99%), ammonium thiocyanate (NH₄SCN, 99%), Te powder (200 mesh, 99.8%, trace metal basis), dimethyl sulfoxide (DMSO, anhydrous, 99.9%), and 1-dodecanethiol (99.8%) were purchased from Sigma Aldrich. Oleic acid (OA, 90%), selenium powder (Se, 200 mesh, 99.999% metal basis), 1-octadecene (ODE, 90%), lead(II) oxide (99.9995%), tris(diethylamino)phosphine ((DEA)₃P, 97%), tetralin (97%), 2,2'-bipyridine (98%), *p*-toluenesulfonyl chloride (99%) and lead (II) bromide (99.999%, metals basis) were purchased from Alfa Aesar. Tetrachloroauric(III) acid trihydrate (99%), sodium oleate (98%), MgSO₄ (98%), Na₂SO₄ (99%), sodium hydroxide (NaOH, 99%), ethylene glycol (99%), silica gel (200–300 mesh), KOH (99%) and 1-methylpiperidin-4-one dichloromethane (98%) were from Innochem. Oleylamine (OLAm, 80–90%), indium (III) chloride (InCl₃, 99.995%) and zinc(II) chloride (>98%) were purchased from Acros. 4-(dimethylamino)pyridine (DMAP, 98%), pyridine (99.5%, extra dry), 4'-bromo-2,2,2-trifluoroacetophenone (98%), trimethylamine (99.5%, extra dry), tetrahydrofuran (THF, 99%, extra dry), isopropyl alcohol (IPA, 99.9%) and iodine (99.8%) were from Energy Chemical. NaN₃ (99%), N'-ethyl-N-(3-(dimethylamino)propyl)carbodiimide hydrochloride (EDC, 99%), 1,1,2-trichloroethane (97%) and deuterated solvents (CDCl₃, 99.8%) were purchased from J&K chemicals. Octane (99%), copper powder (99.5%) and (3-mercaptopropyl)trimethoxysilane (95%) were from Meryer. 1,4-diiodooctfluorobutane (98%), 4-[3-(trifluoromethyl)-3H-diazirin-3-yl]benzyl bromide (95%), 1,1,2,2,3,3,4,4-octafluoro-1,4-diiodobutane (98%) and 2,3,4,5,6-pentafluorobenzaldehyde (96%) were purchased from TCI. Petroleum ether (AR), ethyl acetate (AR) and dichloromethane (AR) were from General Reagent. Hydrochloric acid (37% solution in water), nitric acid solution (65% in water), hydroxylammonium chloride (98%, Greagent), acetone (AR) and chloroform (AR) were purchased from Tongguang Fine Chemicals. Hexane (99.5%) and ethanol (99.5%) were from Fisher. Trioctylphosphine (TOP, 97%) was from Strem. Methyl 2,3,4,5,6-pentafluorobenzoate (97%) was purchased from Heowns. Toluene (99.5%) was purchased from Fisher and purified by using MBraun MB SPS Solvent Manual Purification System. All other chemicals were used as received.

2. Syntheses of nanocrystals (NCs).

All syntheses were performed using conventional air-free techniques including Schlenk lines/flasks and a nitrogen-filled glovebox.

Quantum dots (QDs). II–VI semiconductor QDs with typical core-shell structures and emission in red (CdZnSe/CdZnS/ZnS), green (CdZnSe/ZnSe/ZnS), and blue (CdZnSe/ZnS) colors were provided by TCL inc. The synthesis followed protocols described in ref.^[1] with slight modifications by using typical organic ligands such as OA and 1-octanethiol. These QDs were purified with hexane/ethanol for 1–2 times, redispersed in toluene (60 mg mL⁻¹), and stored under inert atmosphere.

Zinc blende CdSe NCs with solely OA ligands were prepared according to the protocols described by Jasieniak et al. with slight modification.^[2] The stock solution of Se in ODE was prepared by mixing Se powder (0.74 g, 9.4 mmol) in ODE (80 g), followed by degassing at 100 °C for 30 min and heating under nitrogen at 200 °C for 2 h. To a 100 mL three-necked flask were loaded 0.67 mL of Cd(oleate)₂ (0.5 M) and 12 mL of ODE. The mixture was degassed at 100 °C for 1 h and then heated to 260 °C under nitrogen. 3.6 mL of Se–ODE solution was rapidly injected at this temperature. The reaction lasted for 20 min before cooled down to room temperature. NCs were isolated by adding ethanol to the crude solution, followed by centrifugation. NCs were then purified with ethanol/hexane three times and redispersed in toluene at the concentration of 60 mg mL⁻¹. This solution was used to prepare NCs with different purification procedures/washing times.

Wurtzite CdSe NCs with OA and OLAm ligands were synthesized using Cd(oleate)₂ and TOPSe as precursors, following a reported method with slight modifications.^[3] **InP NCs** were synthesized with InCl₃ and (DEA)₃P as precursors.^[4] **PbS NCs** capped with

SUPPORTING INFORMATION

OA ligands were prepared following a previous method.^[6] (γ -Fe₂O₃)_{1-x}(Fe₃O₄)_x NCs were synthesized according to the protocols reported by Hyeon group.^[6] Au NCs with OLAm ligands were prepared at room temperature as reported.^[7] HgTe NCs were prepared with previously reported method.^[8] CsPbBr₃ NCs were obtained via a hot injection approach reported by Kovalenko and co-workers.^[9] Typically, these NCs were purified 3 times with hexane/ethanol and redispersed in toluene, and stored in a glove box (Au NCs were stored at 4 °C). CsPbBr₃ NCs were purified with methyl acetate as the nonsolvent.

3. Synthesis of crosslinkers.

Crosslinker 1 ((1*E*,4*E*)-1,5-bis(4-azido-2,3,5,6-tetrafluorophenyl)penta-1,4-dien-3-one) was synthesized according to reported protocols (**Scheme S1**).^[10] The yellowish powder of **1** was obtained after synthesis and purification. ¹H-NMR (400 MHz, CDCl₃): δ = 7.68 (d, 2H), 7.30 (s, 2H); ¹⁹F-NMR (377 MHz, CDCl₃): δ = -151.71 (m, 4F), -139.24 (m, 4F) (**Figure S1**).

Crosslinker 2 (ethylene bis(4-azido-2,3,5,6-tetrafluorobenzoate)) was synthesized following reported protocols (**Scheme S2**).^[11] **2** was obtained as a white solid. ¹H-NMR (400 MHz, CDCl₃): δ = 4.68 (s, 4H); ¹⁹F-NMR (377 MHz, CDCl₃): δ = -150.61 (m, 4F), -138.06 (m, 4F) (**Figure S2**).

Crosslinker 3 ((3*E*,5*E*)-3,5-bis(4-azido-2,3,5,6-tetrafluorobenzylidene)-1-methylpiperidin-4-one) was synthesized following ref.^[12] (**Scheme S3**). **3** was obtained as an off-white solid. ¹H-NMR (400 MHz, CDCl₃): δ = 2.37 (s, 3H), 3.42 (s, 4H), 7.56 (s, 2H); ¹⁹F-NMR (377 MHz, CDCl₃): δ = -151.30 (m, 4F), -137.06 (m, 4F) (**Figure S3**).

Crosslinker 4 (3,3'-(4,4'-(perfluorobutane-1,4-diyl)bis(4,1-phenylene))bis(3-(trifluoromethyl)-3H-diazirine)) was prepared according to the procedures reported by Simhadri et al.^[13] The syntheses contain five steps as shown in **Scheme S4**. **4** was a shiny white crystal after purification. ¹H-NMR (400 MHz, CDCl₃): δ = 7.59 (d, 4H), 7.29 (d, 4H); ¹⁹F-NMR (377 MHz, CDCl₃): δ = -64.90 (s, 6F), -110.02 (t, 4F), -121.18 (t, 4F) (**Figure S4**).

4. Procedures for direct optical patterning of NCs.

Direct optical patterning of NCs with nitrene- and carbene-based photocrosslinkers was performed under yellow light typically used for cleanroom lighting. The UV light source was either a 254 nm low-pressure mercury vapor grid lamp (BHK Company Inc.) or a handheld UV lamp (254 or 365 nm) purchased from Guangzhou Fusiao Special Lighting Instrument Co., LTD. Photomasks were made by photolithography and wet etching of thin chromium layers on quartz substrates. Substrates for NC patterning included glass, quartz, and Si wafers. These substrates were cleaned by sequential wash of toluene, acetone, methanol, and ethanol (or isopropanol), and dried under a nitrogen flow prior to use. The patterning included three steps, as depicted in Figure 1D, and can be repeated to build multi-layered patterns from the same or different NCs.

i) Film deposition. A solution containing NCs (typically 10–30 mg mL⁻¹, in hexane, octane or toluene) and crosslinkers (up to ~10 wt.% relative to the mass of NCs) was filtered through a 0.2 μ m PTFE filter and spin-coated on a substrate. Typical parameters for spin-coating were spread: 400 rpm, 3 s; spin: 2000 rpm, 30 s. The concentration of NC solution and the spin-coating parameters can be adjusted to control the thickness of patterned NC layers.

ii) UV exposure via a photomask. The NC film was then brought into contact with a predesigned photomask either on a mask aligner (URE-2000/25) or by using binder clips (as described by Wang et al.^[14]). High resolution (feature sizes < 3 μ m) patterns were preferably made with a mask aligner in a 1000 grade cleanroom, while single-layered patterns with lower resolution (5 μ m and above) can be readily obtained in a regular lab environment (yellow light). Typical UV exposure dose ranged from 20–200 mJ cm⁻².

iii) Developing. Toluene, hexane and other common nonpolar solvents were employed as developer to dissolve NCs in the unexposed areas. NC thin films were immersed in developer for ~1 min.

SUPPORTING INFORMATION

In a typical patterning procedure of red-emitting QDs, filtered QD solution in toluene (30 mg mL⁻¹, containing 3 wt.% of crosslinker **1**) was spin-coated on a substrate (spread: 400 rpm, 3 s; spin: 2000 rpm, 30 s). The film was then exposed to 365 nm UV light (dose: 50–100 mJ cm⁻²) via a photomask, followed by soaking in hexane or toluene for ~1 min to remove QDs in the unexposed regions. When patterning QDs with **4**, slightly larger amount of crosslinkers (~6 wt.%) and longer exposure (200–300 mJ cm⁻²) were used. Parameters for NC patterning, including NC concentration, mass ratio of crosslinkers and exposure doses, varied depending on the sizes, shapes, compositions and surface chemistry of NCs.

5. Quantification of patterning capabilities.

Zinc blende CdSe NCs synthesized and capped with only OA ligands, together with crosslinker **1**, were employed as the model system to provide a quantitative evaluation of patterning capabilities. Film retention (%) was defined as, *film retention* = $\frac{\text{mass of remained NCs}}{\text{mass of remained NCs} + \text{mass of developed NCs}} \times 100\%$, where the mass of NCs remained in the film after patterning and developing, and the mass of NCs in the developer were measured by using inductively coupled plasma–optical emission spectroscopy (ICP–OES). In brief, films (coated on a 1.25 × 1.25 cm substrate) containing NCs and photocrosslinkers were exposed under different conditions, as shown in Figure S7. The photopatterned/crosslinked films were immersed in 2 mL of toluene for 3 min and then rinsed with another 1 mL of toluene to thoroughly remove uncrosslinked/poorly crosslinked NCs. The “developed” NCs in toluene was recovered after solvent evaporation. The recovered NC solids were digested in 0.5 mL aqua regia, and diluted for ICP–OES analysis. The measured concentration of Cd element was used to calculate the mass of developed NCs. In parallel, NCs remained in the films were digested with aqua regia and measured by ICP–OES for estimating the mass of remained NCs. Film retention of NCs patterned under various conditions (shown in Figure S7) was calculated accordingly.

The ligand density of purified CdSe NCs with solely OA ligands was calculated based on the results from a combination of characterization techniques. Thermogravimetric analysis (TGA) provided the mass ratio of OA ligands and CdSe NC cores. The sizes of zinc blende CdSe NCs were estimated from UV-visible absorption spectra, following methods described in earlier reports.^[15] Assuming NCs are in spherical shape with uniform size, the ligand density (number of ligands per NC surface area) was calculated (Figure S8). In brief, the diameters of zinc blende CdSe NCs followed the equation of $D = \frac{1280}{(810-\lambda)} - 1.9$, where λ stands for wavelength of the first excitonic absorption peak of NCs. From these, one can calculate the ligand density, number of ligands per NC, and the molar ratio of ligands and crosslinkers, as listed in Figure S8. We also attempted to quantify the ligand density of NCs by using ¹H-NMR spectra with ferrocene as the internal standard. However, the small difference in the amount of OA ligands for NCs purified for 3 and 6 time made this quantification challenging in our case.

6. Fabrication and characterizations of pristine and patterned QLEDs

Pristine and patterned QLED devices were fabricated with a standard structure containing stacked layers of indium tin oxide (ITO)/poly(3,4-ethylenedioxythiophene) polystyrene sulfonate (PEDOT:PSS)/Poly[(9,9-dioctylfluorenyl-2,7-diyl)-alt(4,4'-(N-(4-butylphenyl)))] (TFB)/red-emitting QDs (pristine or patterned)/ZnO/Al. The ITO-coated glass substrates were cleaned sequentially in ultrasonic bath of detergent, de-ionized water, acetone, and isopropanol for 15 min each, and then were immediately exposed to UV ozone for 20 min. PEDOT:PSS solution (Heraeus, Clevios™ P VP.Al 4083) was spin-coated onto the substrates at 5000 rpm and baked at 140 °C for 15 min under ambient atmosphere. The substrates were then transferred to a nitrogen-filled glovebox. The TFB layer (20 nm) was then spin-coated by using the corresponding solution (ADS 259BE, Nichem Fine Technology Co. Ltd., at 3000 rpm, 30 s), followed by annealing at 200 °C for 30 min. The QD layers (25 nm) were spin-coated at 2000 rpm for 30 s and annealed at 80 °C for 10 min. QD layers in pristine devices were coated from a dilute QD solution (10 mg mL⁻¹, 2000 rpm, 30 s), while those in the patterned devices were photocrosslinked with **1**, **2**, or **4**. For simplicity in device performance comparison, the entire area of “patterned” QD layer was exposed to UV under conditions suitable for photocrosslinking, followed by developing in toluene (or octane for crosslinker **4**). Patterned devices with crosslinkers **1** and **2** (5 wt.% relative to the mass of QDs) were exposed (at 254 or 365 nm) for 50 mJ cm⁻² while those with **4** (10 wt.%) were exposed (at 365 nm) for 200 mJ cm⁻². The ZnO layer (35 nm) was spin-coated at 2000 rpm for 30 s and then annealed at 80 °C for 30 min. The devices were then loaded into a high-vacuum deposition chamber (at a pressure of $\leq 1 \times 10^{-6}$

SUPPORTING INFORMATION

mbar) to thermally deposit the Al cathode (100 nm). Finally, the devices were encapsulated by using cover glass with a UV-curable resin. Device performance (EQE, luminance, operating lifetime) of encapsulated devices were measured under ambient atmosphere. EQE and luminance were measured by a combination of QE-PRO spectrograph, Keithley 2400, and Keithley 6485 meters and operating lifetime was measured by Crysco Keitley 3706A.

7. Fabrication and characterizations of other prototype devices

For the conductivity measurements of patterned Au NC films after post-patterning ligand exchange, a mixed solution of Au NCs (30 mg mL⁻¹) and 8 wt.% of crosslinker **1** was spin-coated on quartz substrates (2000 rpm, 30 s). The substrates were cleaned and coated with a self-assembled monolayer of 3-mercaptopropyltrimethoxysilane (MPTS), as described in previous work.^[16] The monolayer coating was achieved by immersing the substrates in a solution of MPTS (5 vol.% in toluene) overnight. This prevented the delamination of NC films, especially during the ligand exchange process. The coated film was exposed to 365 nm UV light for 500 mJ cm⁻² and developed in toluene. For ligand exchange with SCN⁻ ligands,^[16b] the film was immersed in a solution of NH₄SCN (10 mg mL⁻¹ in acetone) for 3 min, followed by washing with acetone twice. The film was then heated to 150 °C for 15 min. These procedures (NC film coating, patterning (UV exposure/developing), ligand exchange and thermal treatment) were repeated twice to obtain a triple layered Au NC film with the thickness of ~50 nm, as estimated by profilometry. For comparison, pristine SCN⁻-treated Au NC films were prepared following similar procedures but without the addition of crosslinkers and the UV exposure/developing steps. The electrical conductivity of both pristine and patterned Au NC films after post-patterning SCN⁻ ligand treatment was measured by Keithley 2400 connected with a probe station, by using the van der Pauw method.

Prototype, pristine and patterned (crosslinked) HgTe NC-based transistors were fabricated by spin-casting HgTe NC solution on Si substrates with pre-defined electrodes. Patterned devices were crosslinked with **2** (3 wt.%) under 254 nm for 100 mJ cm⁻² and developed with toluene. Both pristine and patterned HgTe devices were treated with an EDT/HCl/IPA solution (1:1:50 by volume) for 20 s, as described in ref.^[8] The transfer characteristics were measured by a Keithley 2602B source meter under vacuum at 80 K. The carrier mobility was calculated by using reported methods.^[17]

8. Characterization techniques

Transmission electron microscopy (TEM) images of NCs were taken using a JEOL JEM-2100F microscope at 200 kV. Scanning electron microscopy (SEM) measurements were performed on a Hitachi SU-08010 microscope. Optical microscopic images of NC patterns in bright and fluorescence modes were captured with a Nikon Ni-U microscope. Atomic force microscopy (AFM) images were obtained in ScanAsyst mode using a Bruker Dimension Icon scanning probe microscope. UV-visible absorption spectra of NC solutions were collected using an Agilent Cary 5000 UV-Vis-NIR spectrophotometer in transmission mode. Photoluminescence (PL) measurements for QDs in both solution and film states were carried out on a Horiba FluoroMax Plus spectrometer. The absolute PL quantum yield (PLQY) of QD films on quartz substrates were measured at an excitation wavelength of 405 nm with an integrating sphere. Time-resolved PL decay data were collected by on a Edinburgh FLS 920 combined steady state and fluorescence lifetime spectrometer. Fourier transform infrared (FTIR) spectra were recorded on a Bruker VERTEX 70 spectrometer in the attenuated total reflection (ATR) mode with at least 64 scans at a resolution of 4 cm⁻¹. The samples were prepared by drop-casting concentrated NC dispersions in hexane on the ATR crystal substrate. NMR data were acquired on a JEOL JNM-ECZ400S instrument, operating at 400 MHz for ¹H-NMR and 377 MHz for ¹⁹F-NMR. CDCl₃ was used as a solvent and the chemical shifts were recorded in δ (ppm) based on the residual CHCl₃ resonance (δ = 7.26 for ¹H). The NMR spectra were analyzed with JEOL Delta NMR software. Profilometry of NC patterns were measured using a Bruker Dektak XT instrument. ICP-OES analysis of digested samples was performed on a Varian Vista-MPX spectrometer. TGA data of CdSe NCs was collected using a Mettler Toledo TGA/DSC 1 HT/1600 instrument at a heating rate of 10 °C min⁻¹ under argon flow. Ultraviolet photoemission spectroscopy (UPS) measurements of crosslinkers **1** and **4** were performed on a ThermoFisher Scientific ESCALAB Xi+ spectrometer using a monochromatic He I (21.2 eV) source. The samples were prepared by spin-coating the corresponding crosslinker solution on a gold-coated (50 nm) silicon wafer. The HOMO energy was obtained directly from the UPS results and calculated by the following equation, $E_{HOMO} = h\nu - (E_{cutoff} - E_{onset})$. The LUMO energy was estimated based on the UV-visible absorption spectra and HOMO level of crosslinkers.

SUPPORTING INFORMATION

Supplementary discussion

1. Quantitative analysis on the patterning capabilities of NCs.

We used film retention, defined as the percentage of NCs remained in the crosslinked (patterned) film after solvent developing and measured by ICP–OES, to provide a quantitative estimation of the patterning quality. Film retention is highly reliant on the UV exposure doses, the contents of crosslinkers, and the ratio between crosslinkers and NC ligands. Zinc blende CdSe NCs with solely OA ligands, together with crosslinker **1**, serve as an example for this analysis. As shown in Figure S7, the film retention of crosslinked NC layers containing ~3 wt.% of **1** increases rapidly with the UV doses in the range of 0–50 mJ cm⁻², followed by saturation (film retention ~70%) at higher doses. Crosslinked films exposed to small UV doses show low film retention and pattern quality, while overexposed ones suffer from poor patterning fidelity. Similarly, there exists an optimal weight content of crosslinkers (3–5 wt.% relative to NCs). The dependence of film retention on the contents of crosslinkers can be further related to the molar ratio of crosslinkers and native ligands on NCs. A combination of characterization techniques provides a rough estimation of the ligand density of CdSe NCs with an average diameter of 4.1 nm (Figure S8). Purified CdSe NCs (6 times) show a ligand density of ~3.6 nm⁻², similar to typical values in previous reports and lower than the packing density of crystalline alkane chains (~4.9 nm⁻²).^[18] This corresponds to ~184 ligands per NC. Increased contents of crosslinker **1** (from 1 to 5 wt.%) translate to higher molar ratio of crosslinkers/ligands from ~2 to 10 mol.% (Figure S8). With only 10 mol.% of crosslinkers, crosslinked NC layers show both high film retention (~75%) and high patterning quality.

2. Tentative photochemical interaction of nitrene and carbene radicals with the surface of QDs.

The correlation of PLQY decreases with nitrene generation (Figures 4C and S12) suggests excess nitrene radicals may be detrimental to the photophysical properties of QDs, in line with that conjectured in an earlier report.^[19] One possible origin of this effect entails the conversion of nitrene to benzarine or ketenimine byproducts via side reactions. The relatively low energy barrier from perfluorophenyl nitrene to these byproducts (~8.8 kcal mol⁻¹)^[20] makes this ring expansion reaction unneglectable. A high yield of over 50% was reported for this reaction in solution phase.^[21] These side products were reported to react quickly with bases such as thiols, alcohols and amines.^[22] We thus suspect they might react with the nucleophilic carboxylate or amine ligands originally bound to QD surfaces and create uncoordinated surface traps. By contrast, phenyl carbenes are reluctant to ring expand (energy barrier of ~13–15 kcal mol⁻¹) due to the potential serious distortion of their planarity.^[20, 22] The “closed shell” configuration of singlet carbene radicals endows them with good Lewis philicity.^[23] The use of carbene as Lewis bases/ligands to stabilize Cd²⁺ or Zn²⁺-metal complexes^[24] and passivate II–VI QDs^[25] has been reported. These suggest carbene radicals are able to keep the QD surface coordination intact. Unraveling the nature of the photochemical effects of nitrene-based crosslinkers needs further studies.

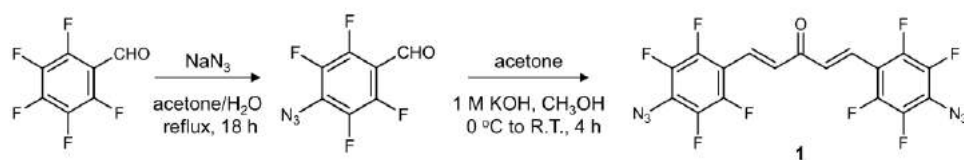
3. Chemical versatility of photocrosslinking based NC patterning

The photocrosslinking patterning approach relies on the reactions between nitrene or carbene radicals and the native surface ligands of NCs. It is insensitive to the NC cores and applicable to a broad range of colloidal NCs with alkyl ligands. Figure S14A–E shows the microscopic images of patterned semiconducting, metallic and magnetic NC layers with **1** under 365 nm. Compared to other direct optical patterning methods,^[26] this approach does not require ligand exchange or polar solvents, and thus adapts well to NCs sensitive to these procedures, such as lead and mercury chalcogenides (PbS, HgTe) and lead halide perovskites (CsPbBr₃).

More interestingly, this approach is compatible with previously reported ligand exchange chemistry for improved electronic communication. The preservation of native ligands with long hydrocarbon chains helps the preservation of the PL and EL characteristics of NCs and the patterning of unstable materials. The presence of these native ligands, on the other hand, impedes the interparticle charge transport in the patterned NC films.^[27] We used ligand exchange strategies developed in previous report to address this issue and found these strategies nicely complement the crosslinking-based patterning method. In brief, soaking patterned NC films in a solution containing short ligands readily replace the native ligands of NCs, even when they are crosslinked. For instance, post-patterning ligand exchange for Au NC films with a solution containing thiocyanate ligands (SCN⁻)^[28] significantly reduces the amount of their native ligands (oleylamine), as evidenced by the diminished C–H vibration peaks (3000–2800 cm⁻¹) in the FTIR spectra (Figure S14F). In

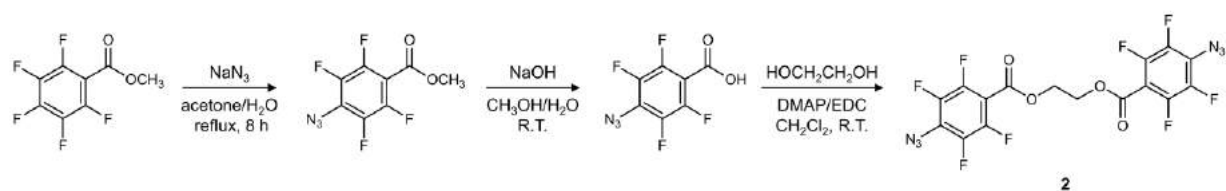
SUPPORTING INFORMATION

addition, the post-patterning treated films show peaks corresponding to SCN^- ($\sim 2200\text{ cm}^{-1}$, shifted to larger wavenumbers due to the strong Au–S bonding) and NH_4^+ (the counter ions of SCN^- , ~ 3200 and 1400 cm^{-1} for N–H), characteristic for SCN^- -capped Au NCs.^[28] This post-patterning ligand exchange process significantly improves the electronic communication in Au NC films, leading to very low electrical resistance ($1.6 \times 10^{-6}\ \Omega\ \text{m}$, Figure S14G) comparable to those of typical SCN^- -treated Au NC films ($0.9 \times 10^{-7}\ \Omega\ \text{m}$). Similarly, the performance of transistors with photocrosslinked HgTe NC layers, followed by ligand exchange with 1,2-ethanedithiol (EDT),^[8] resembles that of typical, pristine devices (Figure S14H). FET measurement is carried out to obtain the electronic properties of the two types of HgTe films. The EDT-treated photocrosslinked HgTe NC films show a similar carrier mobility ($0.08\text{ cm}^2\ \text{V}^{-1}\text{s}^{-1}$) to that of EDT-treated pristine NC films ($0.04\text{ cm}^2\ \text{V}^{-1}\text{s}^{-1}$). These results show the potential of this photocrosslinking approach, after combined with optimized post-patterning ligand exchange chemistry, in building various integrated NC-based devices.



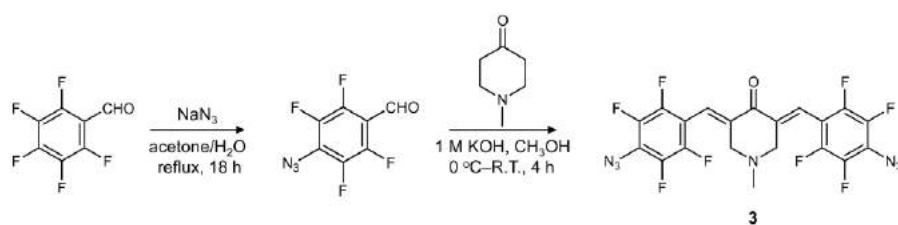
Scheme S1. Synthesis of the crosslinker 1. R.T., room temperature.

SUPPORTING INFORMATION



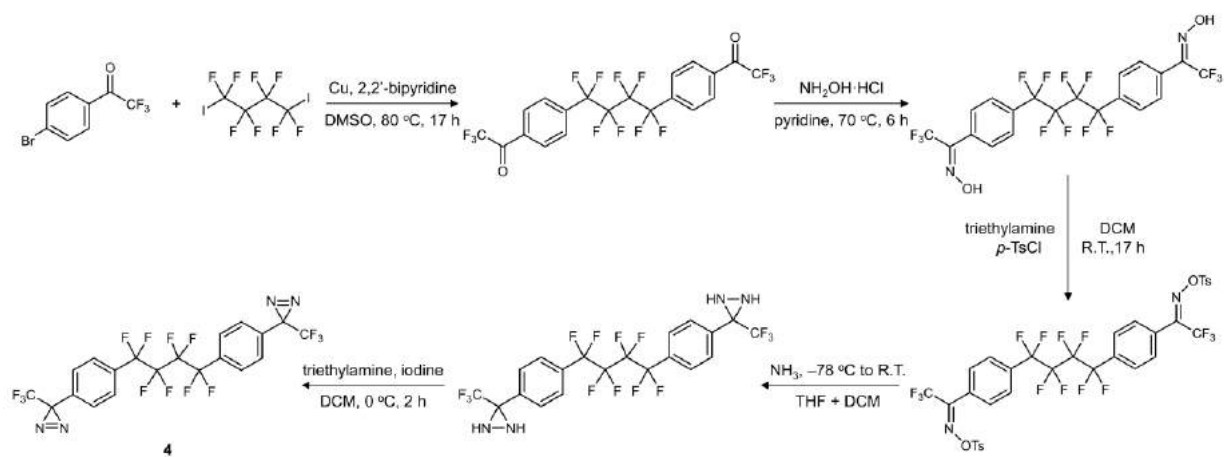
Scheme S2. Synthesis of the crosslinker **2**.

SUPPORTING INFORMATION



Scheme S3. Synthesis of the crosslinker **3**.

SUPPORTING INFORMATION

Scheme S4. Synthesis of the crosslinker **4**.

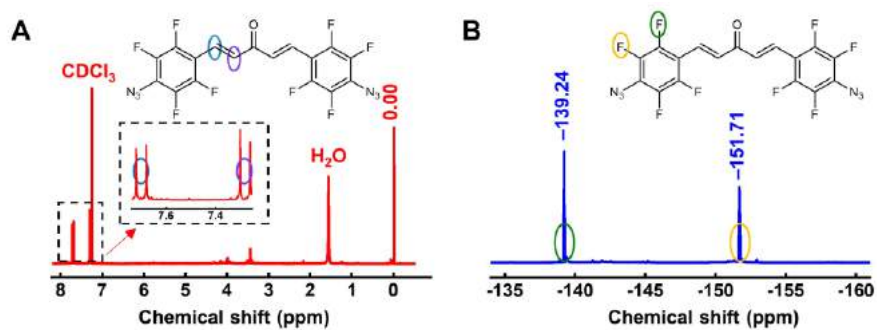


Figure S1. ^1H and ^{19}F -NMR spectra of crosslinker 1 in CDCl_3 .

SUPPORTING INFORMATION

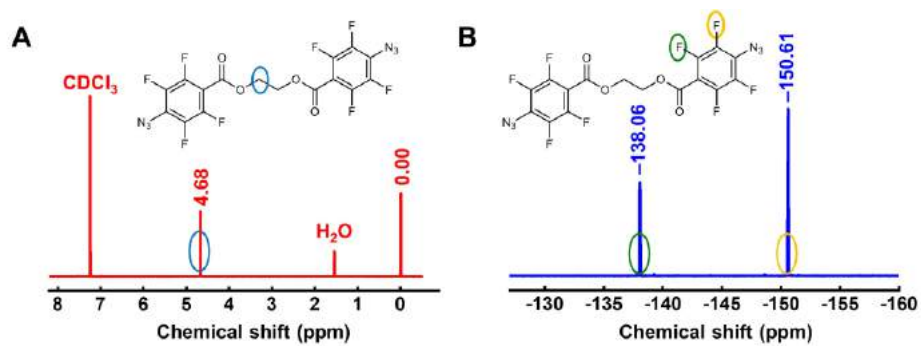


Figure S2. ^1H and ^{19}F -NMR spectra of crosslinker **2** in CDCl_3 .

SUPPORTING INFORMATION

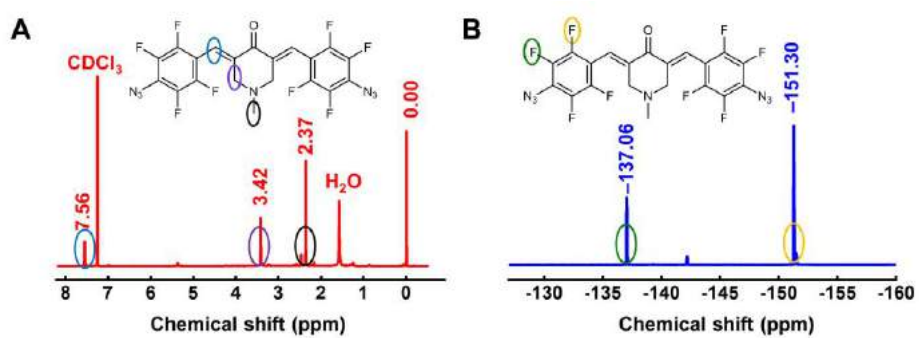


Figure S3. ^1H and ^{19}F -NMR spectra of crosslinker **3** in CDCl_3 .

SUPPORTING INFORMATION

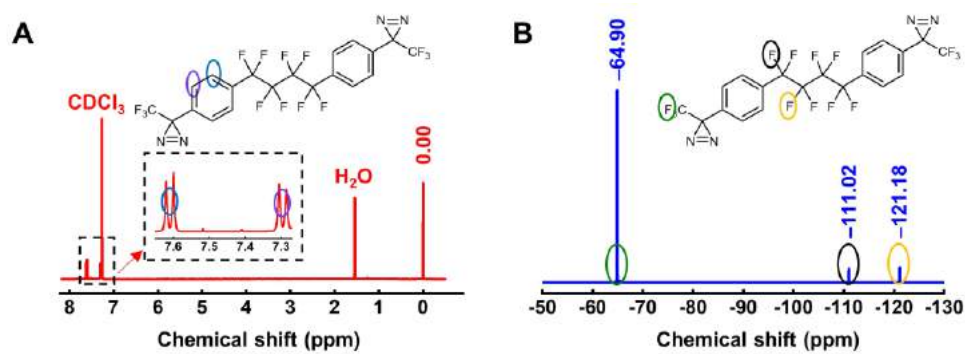


Figure S4. ^1H and ^{19}F -NMR spectra of crosslinker **4** in CDCl_3 .

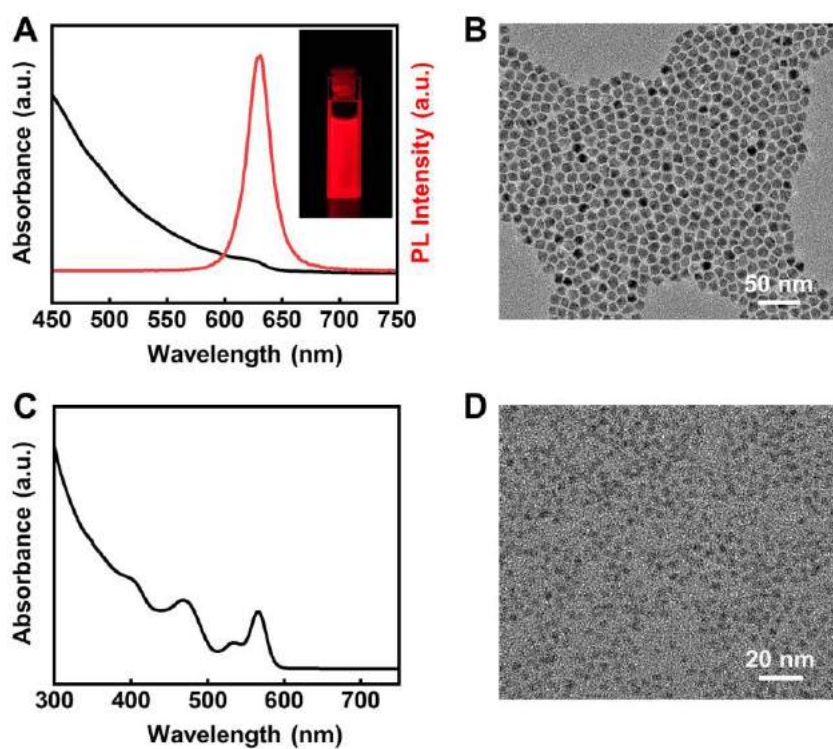


Figure S5. Optical and morphological properties of red-emitting QDs and CdSe NCs. (A,B) UV-visible absorption/PL spectra and TEM image of QDs. (C,D) UV-visible absorption spectrum and TEM image of CdSe NCs. Inset in (A) shows a photograph of QD solution under UV illumination.

SUPPORTING INFORMATION

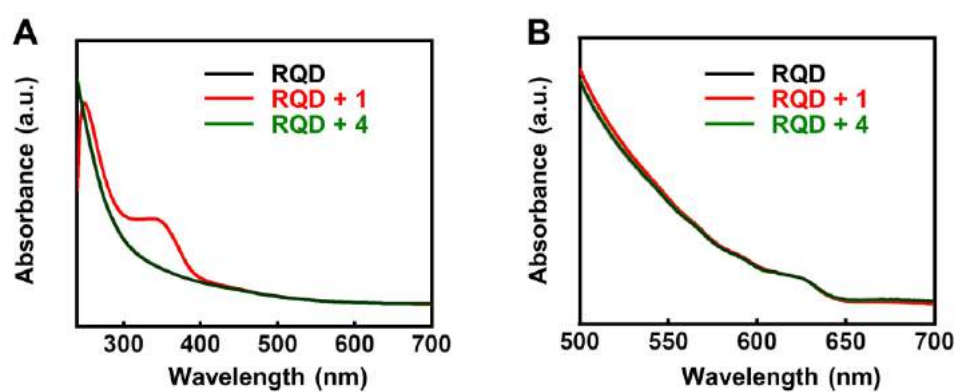


Figure S6. UV-visible absorption spectra of solutions containing red-emitting QDs (RQDs) and crosslinkers. (A) UV-visible absorption spectra of QDs, QDs with 3 wt.% of crosslinker **1** and QDs with 6 wt.% of **4**. (B) Magnified view of (A), highlighting the QD absorption peak at ~625 nm. QDs show high ϵ and the addition of **4** does not introduce notable changes in absorption spectra.

SUPPORTING INFORMATION

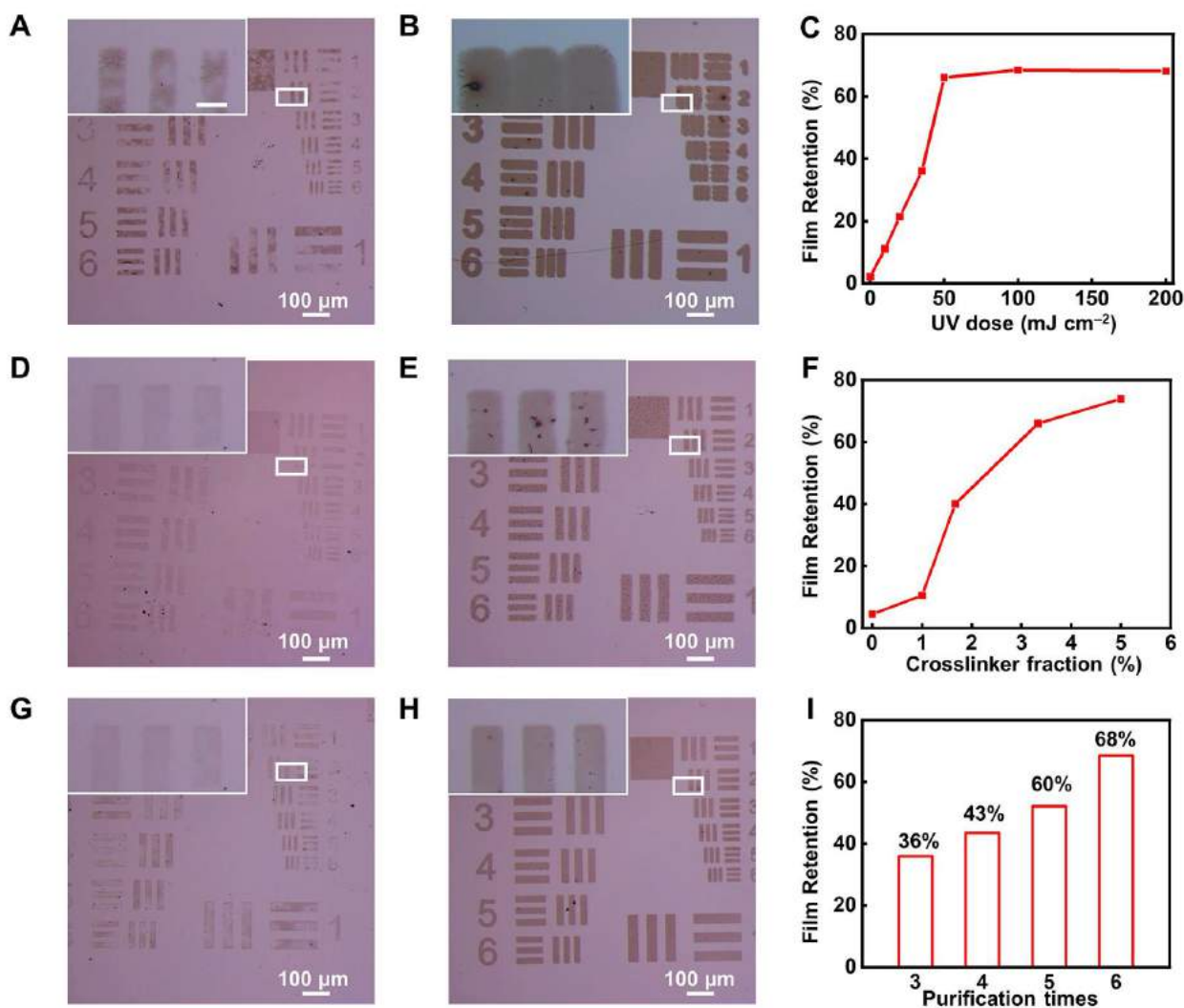


Figure S7. Quantitative relation between film retention and patterning conditions. Oleic acid-capped CdSe NCs patterned (in the format of 1951 U.S. Air Force target) with crosslinker **1** at 365 nm serve as the model system. (A–C) The effect of UV doses. (A,B) Optical images of patterned NC layers with 3 wt.% of **1** and doses of 10 and 200 mJ cm⁻², respectively. (C) Changes in film retention with UV doses. (D–F) The effect of fraction of crosslinkers (weight percentage relative to NCs). (D,E) Optical images of patterned NC layers with insufficient 1 wt.% and excessive 8 wt.% of crosslinker **1**, respectively, for 50 mJ cm⁻². (F) Changes in film retention with crosslinker fraction. (G–I) The effect of ligand coverage of NCs. (G,H) Optical images of patterned NC layers with NCs purified 3 and 6 times, respectively. (I) Changes in film retention with different purification times for CdSe NCs, with 3 wt.% of **1** and 50 mJ cm⁻². Insets in the optical images show the magnified view of areas in the white boxes. Scale bar in inset of A is 20 μm.

SUPPORTING INFORMATION

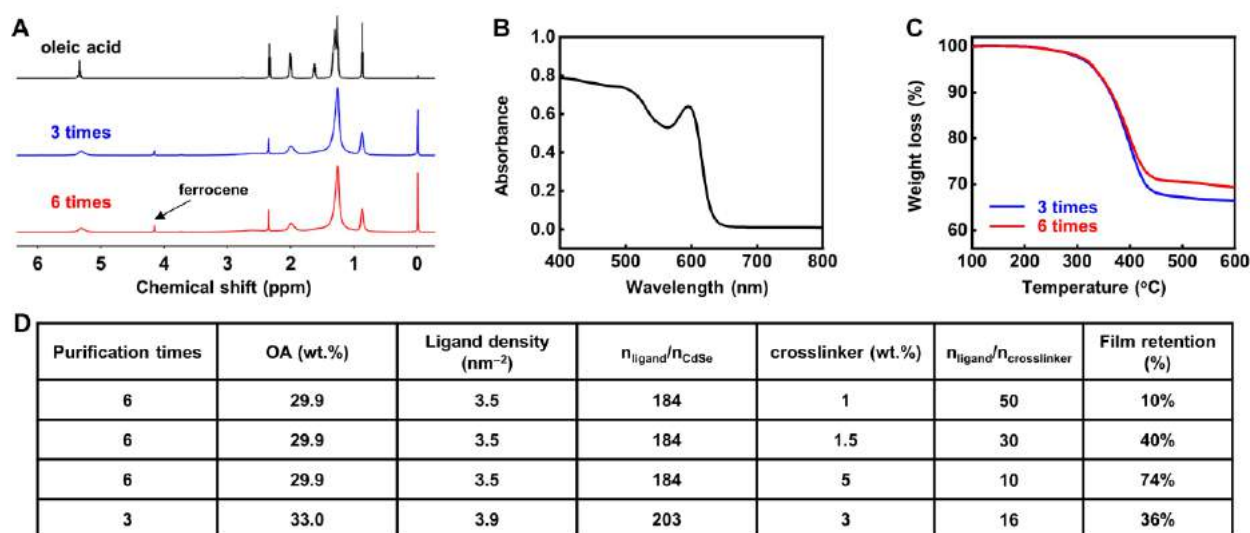


Figure S8. Quantitative analysis of the ligand density of oleic acid capped-CdSe NCs. (A) ¹H-NMR of pure oleic acid and purified NCs (3 and 6 times) in CDCl₃. Ferrocene was added as an internal standard for quantifying ligand concentration. No resonance related to the alkene groups in ODE was observed as a result of NC purification. The precise analysis of ligand concentration is not straightforward due to the small changes in ligand density. (B) UV-visible absorption spectrum of CdSe NCs in toluene, from which the size of concentration of NCs can be estimated. (C) TGA analysis of NCs purified for different times, which provide the concentration of oleic acid ligands. (D) A summary of ligand concentration/density, ratios of the number of ligands (n_{ligand}), number of crosslinkers ($n_{\text{crosslinkers}}$) and number of NCs (n_{CdSe}) and film retention.

SUPPORTING INFORMATION

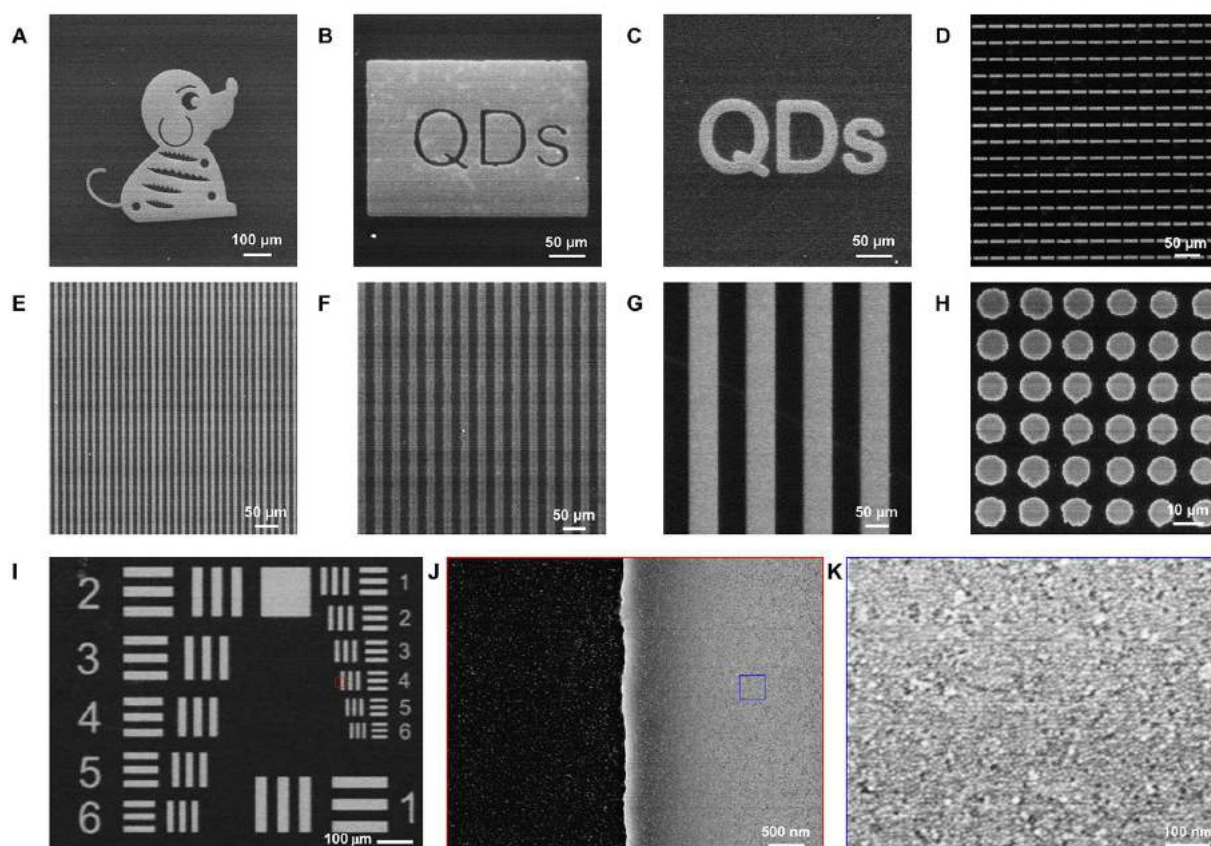


Figure S9. Additional SEM images of QD patterns with **1** at 365 nm. (A–C) QD patterns in the formats of complex patterns and letters, (D–H) patterned arrays of bars, lines and dots, (I) QD layers in the pattern of 1951 U.S. Air Force target. (J) highlights the clean boundary at the edge near the red square in (I) and (K) shows a magnified, uniform patterned layer in the blue square region in (J).

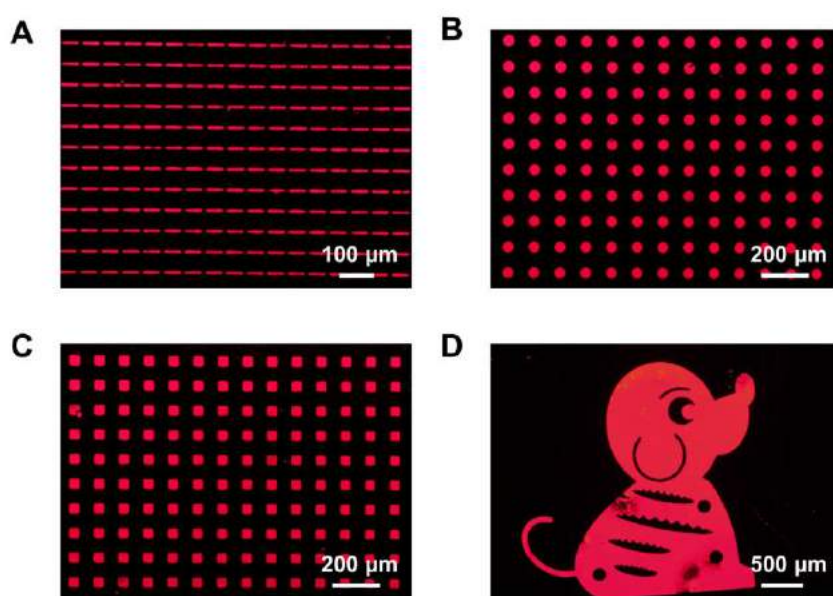


Figure S10. Fluorescence optical microscopic images of patterned QDs formed with crosslinker 4. Typical patterning uses 6 wt.% of crosslinker 4 and a dose of 200 mJ cm^{-2} at 365 nm.

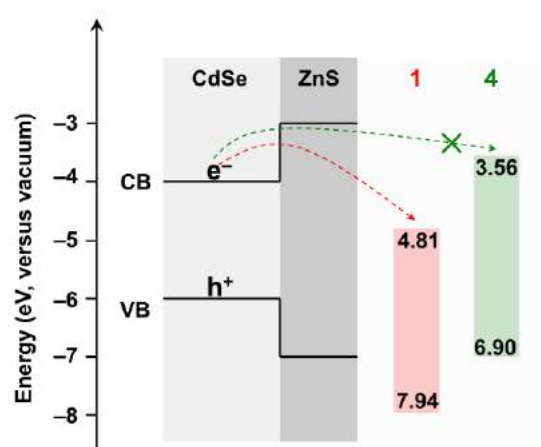


Figure S11. Schematic energy level of red QDs (with approximate CdSe/ZnS structures for simplicity) and crosslinkers **1** and **4**. The edges of conduction band (CB) and valence band (VB) for QDs are from ref.^[29] The HOMO and LUMO levels of **1** and **4** are estimated based on their UPS and UV-visible absorption spectra. The energy level alignments suggest **1** may accept electrons from QDs while **4** can hardly trap electrons or excitons.

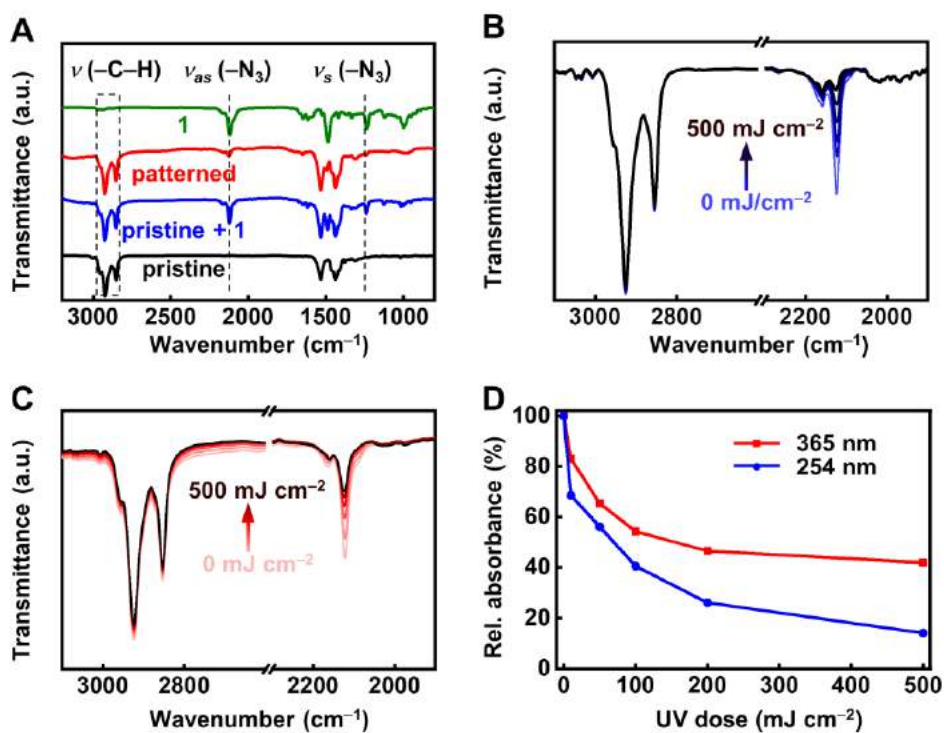


Figure S12. Changes in FTIR spectra during the patterning process of oleic acid-capped CdSe NCs with 1 at 254 or 365 nm. (A) FTIR spectra of 1, pristine NC films, pristine NC films with the addition of 1, and patterned films. The vibrational modes at ~ 2100 and 1300 cm^{-1} correspond to the asymmetric and symmetric stretching of azido groups ($-\text{N}_3$). (B,C) Changes in FTIR spectra of NC films with increased UV doses at (B) 254 and (C) 365 nm. (D) Normalized relative absorbance of $\nu_{as}(-\text{N}_3)$ as a function of UV doses at 365 and 254 nm.

SUPPORTING INFORMATION

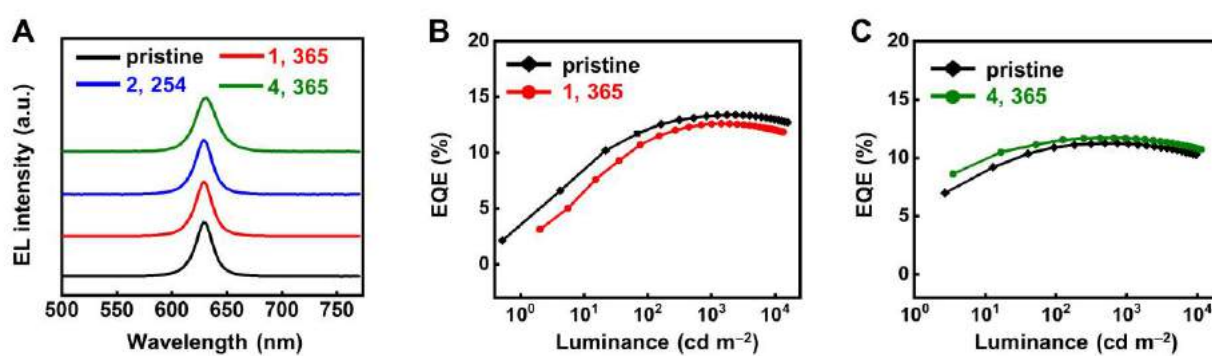


Figure S13. EL characteristics of patterned QLEDs. (A) EL spectra of QLEDs with different patterning conditions (pristine, patterning with 1 at 365 nm, with 2 at 254 nm, and with 4 at 365 nm). (B,C) EQE characteristics of pristine and 365 nm-patterned devices with crosslinkers 1 and 4. Note data in (B,C) were obtained from two batches of devices and corresponding pristine devices are used for comparison. Nonetheless, the typical EQEs of pristine devices for both batches are around 11–13%.

SUPPORTING INFORMATION

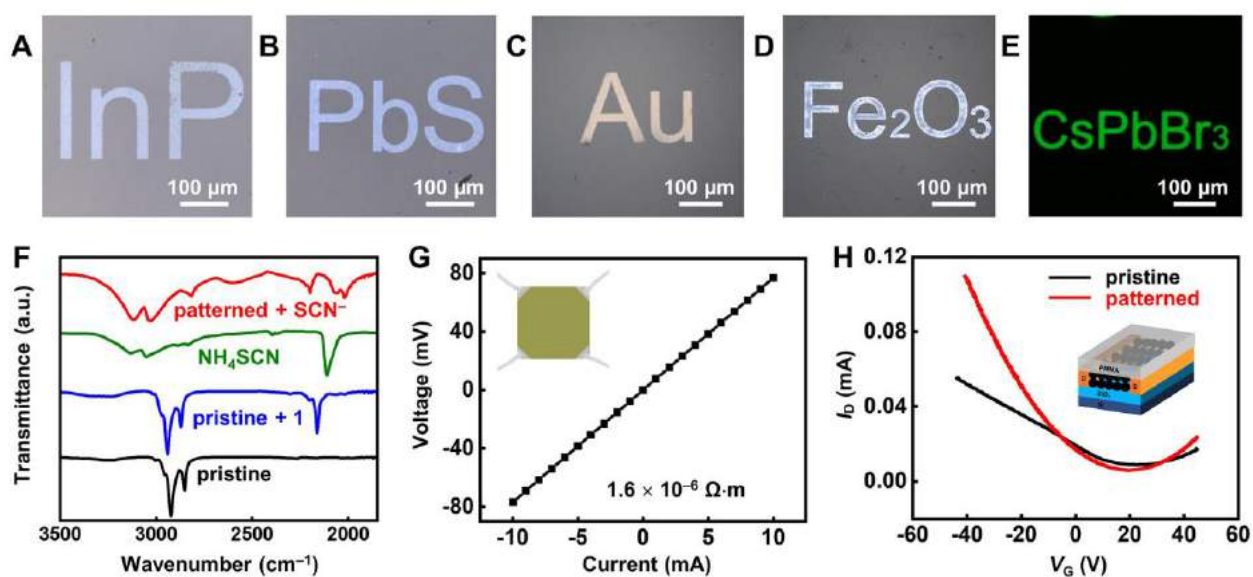


Figure S14. Direct optical patterning of various NCs toward different device structures with photocrosslinkers. (A–E) Optical images of patterned layers of different types of NCs (their identities are shown in the patterns) with **1** at 365 nm. (F) FTIR spectra of pristine oleylamine-capped Au nanoparticle films, after addition of **1** (pristine + **1**), and patterned films after ligand exchange with SCN⁻. The spectrum of NH₄SCN (green curve) is provided for comparison. (G) I–V curve of patterned Au NC films after ligand exchange with SCN⁻ measured by van der Pauw configuration. (H) Transfer characteristics of a prototype device with transistor configuration and pristine or photocrosslinked HgTe NCs as active layers, followed by ligand exchange with EDT. $V_{DS} = 3.0$ V. Insets in (G,H) show schemes of device configurations for conductivity and mobility measurements.

SUPPORTING INFORMATION

Table S1. Fitting parameters for time-resolved PL of thin films of red emitting QDs and calculated rates for radiative (k_r) and nonradiative (k_{nr}) recombination events under different patterning conditions with crosslinker 1, including pristine, formulation (+1), UV exposure (+365 or 254 nm), and patterning (+1 + 365 nm and +1 + 254 nm). τ_{avg} is the abbreviation of averaged lifetime.

Sample	τ_{avg} (ns)	τ_1 (ns)	A ₁ (%)	τ_2 (ns)	A ₂ (%)	PLQY (%)	k_r (μs^{-1})	k_{nr} (μs^{-1})
pristine	21.1	12.8	87.4	78.4	12.6	53	25	22
+ 1	17.1	12.2	87.9	52.8	12.1	45	26	32
+ 365 nm	20.2	12.5	88.6	80.5	11.4	51	25	24
+ 1 + 365 nm	15.1	10.6	87.9	47.2	12.1	29	19	47
+ 254 nm	17.4	11.6	90.0	69.8	10.0	31	18	40
+ 1 + 254 nm	13.5	9.7	86.2	37.3	13.8	20	15	59

The k_r and k_{nr} were calculated by using the following equation^[30].

$$PLQY = \frac{k_r}{k_r + k_{nr}} = \tau_{avg} \times k_r$$

SUPPORTING INFORMATION

Table S2. Summary of EL characteristics of pristine and patterned QLED devices. Patterned devices include those with **1** and **2** at 365 or 254 nm, and those with **4** at 365 nm. The characteristics of patterned devices were compared to those of corresponding pristine ones. The operational lifetime was provided in the forms of measured T_{95} and estimated $T_{95@1k}$ nit.

Devices	EQE (%)	$L@6V$ (cd m^{-2})	T_{95} (h)	$T_{95@1k}$ nit (h)
pristine ^[a]	13.4	15750	96.7	3679
1, 365 nm	12.6	6693	52.9	1823
1, 254 nm	11.6	6267	47.9	1459
2, 254 nm	12.2	5064	44.2	1429
pristine ^[b]	11.2	9628	198.9	4103
4, 365 nm	11.7	11330	191.6	4852

[a] pristine device for patterned devices with nitrene-based crosslinkers.

[b] pristine device for patterned devices with carbene-based crosslinkers.

SUPPORTING INFORMATION

References

- [1] C. Xiang, L. Wu, Z. Lu, M. Li, Y. Wen, Y. Yang, W. Liu, T. Zhang, W. Cao, S. W. Tsang, B. Shan, X. Yan, L. Qian, *Nat. Commun.* **2020**, *11*, 1646.
- [2] J. Jasieniak, C. Bullen, J. van Embden, P. Mulvaney, *J. Phys. Chem. B* **2005**, *109*, 20665–20668.
- [3] B. Mahler, N. Lequeux, B. Dubertret, *J. Am. Chem. Soc.* **2009**, *132*, 953–959.
- [4] M. D. Tessier, K. De Nolf, J. De Roo, Z. Hens, *Chem. Mater.* **2015**, *27*, 4893–4898.
- [5] M. A. Hines, G. D. Scholes, *Adv. Mater.* **2003**, *15*, 1844–1849.
- [6] J. Park, K. An, Y. Hwang, J. G. Park, H. J. Noh, J. Y. Kim, J. H. Park, N. M. Hwang, T. Hyeon, *Nat. Mater.* **2004**, *3*, 891–895.
- [7] S. Peng, Y. Lee, C. Wang, H. Yin, S. Dai, S. Sun, *Nano Research* **2008**, *1*, 229–234.
- [8] X. Tang, M. M. Ackerman, M. Chen, P. Guyot-Sionnest, *Nat. Photon.* **2019**, *13*, 277–282.
- [9] L. Protesescu, S. Yakunin, M. I. Bodnarchuk, F. Krieg, R. Caputo, C. H. Hendon, R. X. Yang, A. Walsh, M. V. Kovalenko, *Nano Lett.* **2015**, *15*, 3692–3696.
- [10] M. Yan, S. X. Cai, M. Wybourne, J. F. Keana, *J. Mater. Chem.* **1996**, *6*, 1249–1252.
- [11] a) J. F. W. Keana, S. X. Cai, *J. Org. Chem.* **1990**, *55*, 3640–3647; b) M. Sundhoro, J. Park, B. Wu, M. Yan, *Macromolecules* **2018**, *51*, 4532–4540.
- [12] D. W. Y. Teo, Z. Jamal, Q.-J. Seah, R.-Q. Png, L.-L. Chua, *J. Mater. Chem. C* **2020**, *8*, 253–261.
- [13] C. Simhadri, L. Bi, M. L. Lepage, M. Takaffoli, Z. Pei, S. F. Musolino, A. S. Milani, G. A. DiLabio, J. E. Wulff, *Chem. Sci.* **2021**, *12*, 4147–4153.
- [14] Y. Wang, J.-A. Pan, H. Wu, D. V. Talapin, *ACS Nano* **2019**, *13*, 13917–13931.
- [15] J. Li, J. Chen, Y. Shen, X. Peng, *Nano Research* **2018**, *11*, 3991–4004.
- [16] a) A. T. Fafarman, S.-H. Hong, S. J. Oh, H. Caglayan, X. Ye, B. T. Diroll, N. Engheta, C. B. Murray, C. R. Kagan, *ACS Nano* **2014**, *8*, 2746–2754; b) A. T. Fafarman, S.-H. Hong, H. Caglayan, X. Ye, B. T. Diroll, T. Paik, N. Engheta, C. B. Murray, C. R. Kagan, *Nano Lett.* **2013**, *13*, 350–357.
- [17] X. Lan, M. Chen, M. H. Hudson, V. Kamysbayev, Y. Wang, P. Guyot-Sionnest, D. V. Talapin, *Nat. Mater.* **2020**, *19*, 323–329.
- [18] a) N. C. Anderson, P. E. Chen, A. K. Buckley, J. De Roo, J. S. Owen, *J. Am. Chem. Soc.* **2018**, *140*, 7199–7205; b) N. C. Anderson, M. P. Hendricks, J. Choi, J. S. Owen, *J. Am. Chem. Soc.* **2013**, *135*, 18536–18548.
- [19] J. Yang, D. Hahm, K. Kim, S. Rhee, M. Lee, S. Kim, J. H. Chang, H. W. Park, J. Lim, M. Lee, H. Kim, J. Bang, H. Ahn, J. H. Cho, J. Kwak, B. Kim, C. Lee, W. K. Bae, M. S. Kang, *Nat. Commun.* **2020**, *11*, 2874.
- [20] N. P. Gritsan, A. D. Gudmundsdóttir, D. Tigelaar, Z. Zhu, W. L. Karney, C. M. Hadad, M. S. Platz, *J. Am. Chem. Soc.* **2001**, *123*, 1951–1962.
- [21] S. X. Cai, D. J. Glenn, M. Kanski, M. N. Wybourne, J. F. W. Keana, *Chem. Mater.* **1994**, *6*, 1822–1829.
- [22] W. T. Borden, N. P. Gritsan, C. M. Hadad, W. L. Karney, C. R. Kemnitz, M. S. Platz, *Acc. Chem. Res.* **2000**, *33*, 765–771.
- [23] a) S. Henkel, P. Costa, L. Klute, P. Sokkar, M. Fernandez-Oliva, W. Thiel, E. Sanchez-Garcia, W. Sander, *J. Am. Chem. Soc.* **2016**, *138*, 1689–1697; b) A. H. Raut, P. Costa, W. Sander, *Chemistry* **2018**, *24*, 18043–18051.
- [24] H. Bauer, L. Orzechowski, A. Escalona, G. Jansen, S. Harder, *Organometallics* **2017**, *36*, 4883–4890.
- [25] a) L. Du, N. A. Nosratabad, Z. Jin, C. Zhang, S. Wang, B. Chen, H. Mattoussi, *J. Am. Chem. Soc.* **2021**, *143*, 1873–1884; b) D. E. Westmoreland, R. Lopez-Arteaga, E. A. Weiss, *J. Am. Chem. Soc.* **2020**, *142*, 2690–2696.
- [26] Y. Wang, I. Fedin, H. Zhang, D. V. Talapin, *Science* **2017**, *357*, 385–388.
- [27] a) C. R. Kagan, C. B. Murray, *Nat. Nanotechnol.* **2015**, *10*, 1013–1026; b) M. A. Boles, D. Ling, T. Hyeon, D. V. Talapin, *Nat. Mater.* **2016**, *15*, 141–153; c) H. Zhang, J. Jang, W. Liu, D. V. Talapin, *ACS Nano* **2014**, *8*, 7359–7369; d) H. Zhang, J. M. Kurley, J. C. Russell, J. Jang, D. V. Talapin, *J. Am. Chem. Soc.* **2016**, *138*, 7464–7467.
- [28] A. T. Fafarman, W.-K. Koh, B. T. Diroll, D. K. Kim, D.-K. Ko, S. J. Oh, X. Ye, V. Doan-Nguyen, M. R. Crump, D. C. Reifsnnyder, C. B. Murray, C. R. Kagan, *J. Am. Chem. Soc.* **2011**, *133*, 15753–15761.
- [29] H. Zhu, N. Song, T. Lian, *J. Am. Chem. Soc.* **2010**, *132*, 15038–15045.
- [30] S. Jin, R. D. Harris, B. Lau, K. O. Aruda, V. A. Amin, E. A. Weiss, *Nano Lett.* **2014**, *14*, 5323–5328.

Author Contributions

S.L. and Z.F. contributed equally to this work. H.Z. conceived the concept of this work. H.Z., S.L. and Z.F. designed the experiments, analyzed the data and co-wrote the paper. S.L. and Z.F. led the experimental work with support from F.L., K.W., L. Zhou, L. Zhang, Y.Y., H.Q., D.L., W.Q., H.D., X.S., M.C., X.T. and L.D. L. Zhou prepared and characterized LED devices and analyzed related data under the supervision of W.L., L.W., and Y.Y. K.W. tested the preliminary LED devices under the supervision of L.D. H.Z. and J.L. supervised the project. All authors discussed the results and commented on the manuscript.